Steroid hormone-induced wingless ligands tune female intestinal size in Drosophila

Lisa Zipper (lisa.zipper@hhu.de)
Heinrich Heine University

Bernat Corominas Murtra (bernat.corominas-murtra@uni-graz.at)
Institute of Biology of the University of Graz

Tobias Reiff (reifft@hhu.de)
Heinrich Heine University https://orcid.org/0000-0001-6610-6148

Article

Keywords:

Posted Date: November 28th, 2023

DOI: https://doi.org/10.21203/rs.3.rs-3500287/v1

Additional Declarations: There is **NO** Competing Interest.

Steroid hormone-induced wingless ligands tune female intestinal size in *Drosophila*

Lisa Zipper, Bernat Corominas Murtra & Tobias Reiff

Abstract (150 words)

Female reproduction comes at great expense to energy metabolism compensated by extensive organ adaptations including intestinal size. Upon mating, *Drosophila* ovaries release the steroid hormone Ecdysone that stimulates a 30% net increase of absorptive epithelium by intestinal stem cell (ISC) divisions. Here, we uncover the transcription factor *crooked legs (crol)* as intraepithelial coordinator of Ecdysone-induced ISC mitosis by establishing Rapport, the first spatiotemporally-controlled dual expression and tracing system for the analysis of paracrine effects on ISC behaviour. Rapport tracing revealed that Ecdysone-induced Crol controls mitogenic Wnt/wg-ligand release from epithelial enterocytes towards ISC, which is counterbalanced by Crol-repression of *string/CDC25* and *Cyclin-B* directly in ISC. Rapport-based ISC tumours confirm paracrine stimulation through the Ecdysone-Crol-Wg axis on mitotic behaviour. Finally, mathematical modelling corroborates increasing enterocyte numbers and Wnt/wg-degradation to set a stable post-mating intestinal size. Together, our findings provide insights into complex endocrine growth control mechanisms during mating-induced adaptations and gastrointestinal cancer.

Introduction

Generation of offspring is an energetically costly process that triggers multiple physiological adaptations of organs such as liver, pancreas and gastrointestinal tract in various species[1,2]. Survival and fitness of progeny relies on tight control of alimentary tract adaptations to metabolic demands in small rodents, in which daily food uptake during lactation can equal the mother´s body weight[1,3]. It is key to understand regulatory mechanisms for hyperplasia and -trophy of the intestine, as it underlies both, physiological tissue functionality and potential malfunctioning in common diseases such as diabetes, obesity and cancer. Physiological adaptations to mating and pregnancy offer a unique opportunity to explore the nature of the underlying interorgan communication.

In *Drosophila melanogaster* females, gut size is increased to match energy consumption when egg production is initiated[4-8]. Endocrine interorgan communication orchestrates this organ size re-set yielding an enlarged intestine with about a third more absorptive enterocytes (EC)[7,8]. This expansion is orchestrated by systemic release of juvenile hormone (JH) from the neuroendocrine corpora allata and the steroid hormone 20-Hydroxy-Ecdysone (20HE) from the ovaries. Both hormones converge on intestinal progenitors increasing intestinal stem cell (ISC) proliferation and enteroblast (EB) differentiation towards EC fate[4,7-10]. 20HE-dependent increases in ISC proliferation depend on presence of the Ecdysone-receptor (EcR) and early response genes *Broad, Eip75B* and *Hr3*[4,8], but mating-dependent molecular control mechanisms of how active 20HE-signalling affects the cell cycle in ISC, remained unknown.

Here, we report and characterize a novel molecular player *crooked legs* (*crol*)/*ZNF267* that relays endocrine 20HE into local intraepithelial ISC division control. We detected 20HE-dependent *crol* activation in ISC and epithelial EC. Interestingly, functional experiments revealed antagonizing mitogenic effects of *crol* manipulation in the ISC population on one hand and the EC population on the other hand. This observation prompted us to design and establish ‘Rapport’, a bipartite spatiotemporally controlled dual binary tracing and expression system, which enabled us to manipulate EC while tracing non-autonomous effects on labelled stem cell progeny. We designed Rapport to offer highest flexibility and compatibility with existing genetic tools and combined it with a driver for epithelial enterocytes. Using Rapport, we discover that Crol relays systemic 20HE signalling in ECs into locally acting paracrine Wnt/Wg ligands. This finding is of high interest as EC are the largest cell population in the midgut and Wnt/wg signalling pathway is central in homeostasis and malignancies of the fly and mammalian gut[11 12]. Manipulation of the 20HE-Crol-Wg axis in microenvironmental EC non-autonomously controls ISC proliferation during mating-dependent intestinal growth and in neoplastic tumours. Quite the contrary, *crol* expression in ISC acts antiproliferative through the CDC25-orthologue *string* and the mitotic cyclin *CyclinB*, suggestive for a Crol-dependent mitotic balance.

Mathematical modelling supports our hypothesis of opposing autonomous and non-autonomous mitogenic effects of Crol on ISC and that EC numbers are indeed stabilizing mating-adapted organ size depending on 20HE levels. Interestingly, our discovered dynamic pattern is highly robust and can be derived from the fundamental properties of diffusion and degradation of Wnt/wg ligands. These

opposing cell type-dependent consequences of a single hormonal stimulus on stem cell proliferation inside the same epithelium underpin complex hormonal action on epithelial growth during pregnancy-induced hyperplasia and pleiotropic effects observed in cancer of the intestine.

Results

Crooked legs responds to mating-dependent 20HE steroid hormone release

The female fly intestine undergoes a variety of post-mating adaptations including a net increase of the absorptive epithelium[5-7]. Mating-dependent enteroplasticity is orchestrated by two hormones, JH and 20HE, which act directly on ISC mitosis[4,7,8]. Aiming to elaborate Ecdysone-responsive genes exerting ISC division control, we followed leads from developmental studies[13-15] and sequencing

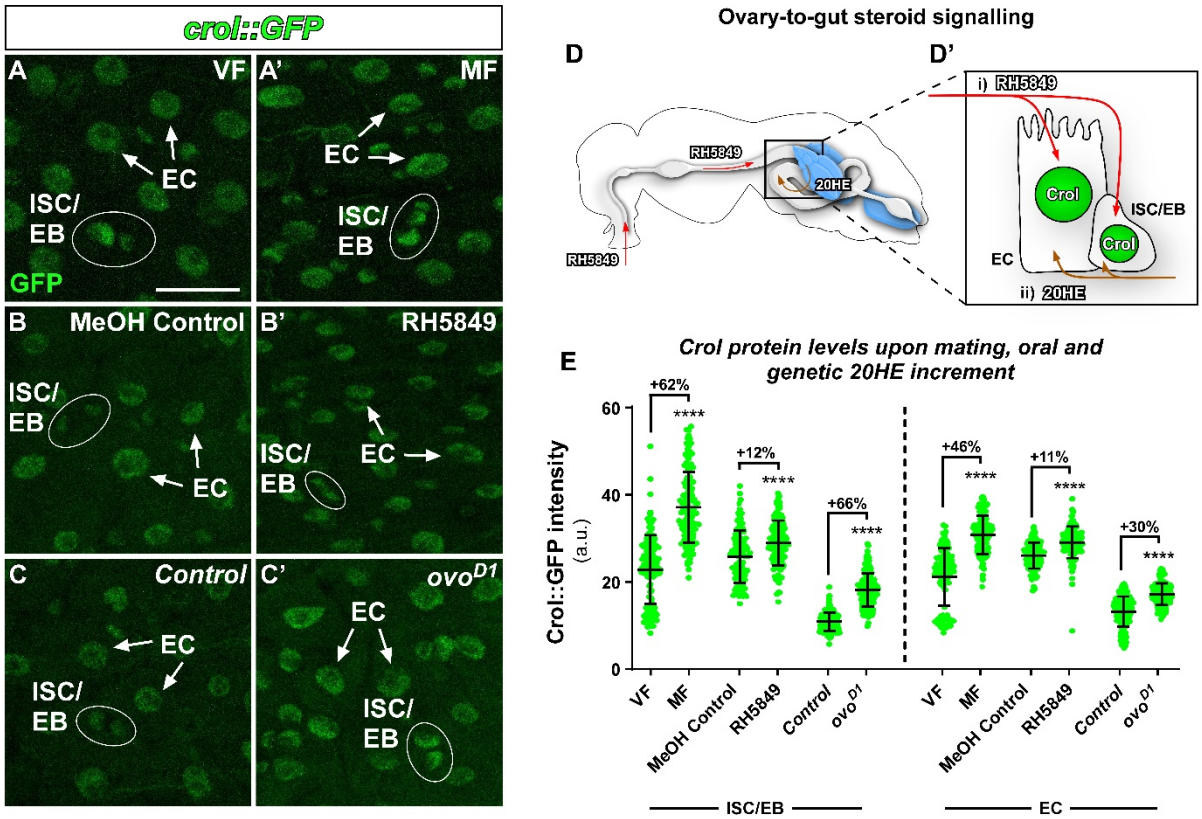

Fig.1: Crooked legs responds to 20HE steroid hormone release

(A-C') Confocal images showing GFP-tagged crooked legs (Crol::GFP) in adult midguts of (A) virgin female (VF) flies compared to (A') mated female (MF) flies, (B) MF fed with MeOH (MeOH Control) compared to (B') MF fed with 20HE agonist RH5849 diluted in MeOH, and (C) MF w^{1118} flies (Contol) compared to (C') heterozygous ovo^{D1} mutant MF. Duplets of stem- and progenitor cells (ISC/EB) are outlined by white ellipses and EC are marked with white arrows. Scale bar is 20µm. (D-D') Schematic of a female fly including midgut and ovaries. The 20HE agonist RH5849 is administrated orally and i) absorbed from the midgut lumen into ISC/EB and EC, whereas 20HE is produced in ovaries and released into the hemolymph ii) from where it is imported into midgut cells. (E) Quantifications of Crol::GFP intensities in ISC/EB and EC upon 20HE levels increased by mating (VF compared to MF), oral administration of 20HE agonist RH5849 (MeOH Control compared to RH5849), and genetical ablation of ovaries by ovo^{D1} mutant allele (*Control* compared to ovo^{D1}). Fold changes are shown in percentages, means and standard deviations are indicated by vertical lines (n=120,120,78,91,178,168/120,120,78,91,198,168). Asterisks denote significances from student's t-test (**p<0.01, ****p<0.0001).

approaches that suggested expression of *crooked legs* in the adult *Drosophila* midgut[16,17].

Transgenic flies in which Crol is GFP-tagged (Crol::GFP) confirmed *crol*-expression in the adult female midgut. We detected GFP-signal in ISC positive for the Notch-ligand Delta (N and Dl, Fig.S1A-A''), in EB identified by N-activity (N-reporter GBE+Su(H)-dsRed, Fig.S1B-B''), in EE positive for Pros (Prospero, Fig.S1C-C'') and EC, positive for the septate junction marker Dlg1 (Discs-large-1, Fig.S1C-C''). Mating induces ovary-to-gut 20HE release[8] and also significantly increased Crol::GFP levels in adult mated females (MF) compared to virgins (VF) (Fig.1A-A',E). Next, we confirmed *crol* responsiveness to pharmacological EcR activation by feeding the EcR agonist RH5849 (Fig.1D-D')[8], which significantly increased Crol::GFP fluorescence intensity compared to controls (Fig.1B-B',E). Similar increases in Crol::GFP fluorescence were observed upon genetic ovariectomy using the dominant *ovoD1* stock (Fig.1C-C',E) abolishing the ovaries as a sink for 20HE[8,18]. Interestingly, *crol* responded in both, ISC/EB as well as epithelial EC populations (Fig.1A-C',E). To investigate the role for *crol* in intestinal tissue homeostasis, we separately addressed its role in ISC/EB progenitors and epithelial EC (Fig.1D').

Crol and its functional human orthologue ZNF267 control proliferation of intestinal stem cells

First, we manipulated *crol* autonomously in ISC and EB using the *'ReDDM'* (Repressible Dual Differential Marker, Fig.S2A) tracing method to observe overall impact on tissue renewal with spatiotemporal control of tracing onset and gene manipulation[19]. Briefly, *ReDDM* differentially marks cells having active or inactive *Gal4* expression with fluorophores of different stability. Combined with the enhancer trap *esg-Gal4,* active in progenitors (ISC and EB), *esg^{ReDDM}* double marks ISC and EB driving the expression of *UAS-CD8::GFP* (*>CD8::GFP*, '>' abbreviates Gal4/UAS regulation and '>>' lexA/AoP regulation in the following) with short half-life and *>H2B::RFP* with long half-life. Upon epithelial replenishment, newly differentiated EC and EE stemming from ISC divisions retain an RFP^{+}-nuclear stain due to fluorophore stability[19]. Crosses are grown at 18°C in which transgene expression is repressed by ubiquitous tubulin-driven temperature sensitive Gal80^{ts}. By shifting adult females to 29°C, Gal80^{ts} is destabilized, in turn enabling temporal control of *esg^{ReDDM}*-tracing and additional UAS-driven transgenes in progenitors (Fig.S2A).

After seven days of tracing adult female intestines using *esg^{ReDDM}*, we found that overexpression of *crol* has an antiproliferative effect decreasing the number of progenitor cells (Fig.2B) about 12-fold (Fig.2E) compared to controls (Fig.2A). Reciprocally, RNAi-knockdown (Fig.2C) and guideRNA (gRNA) mediated excision of *crol* (Fig.S2F) using *esg^{ReDDMCas9}* tracing significantly increased the number of progenitors (Fig.2D, S2G), new epithelial cells (Fig.S2H) and stimulated ISC division (Fig.S2I) compared to controls (Fig.S2B). Similar results were obtained using independent overexpression and loss-of-function transgenics of *crol* (Fig.S2C-I). Underlining functionality of both, the reporter and RNAi stock, *crol-RNAi* driven by *esg>* in ISC and EB reduces Crol::GFP fluorescence (Fig.S2J-L'').

We next sought to identify human orthologues of *crooked legs* and by mining databases for zinc finger transcription factors with a high degree of sequence homology to Crol, we isolated the human Krüppel-like zinc finger transcription factor ZNF267. To explore the ability of human ZNF267 to substitute Crol function in intestinal progenitors, we depleted endogenous crol by RNAi and expressed human ZNF267 at the same time (Fig.2D) and observed rescue of *crol-RNAi*-induced progenitor accumulations by ZNF267 (Fig.2D-E). In line with these observations, ZNF267 regulates cell proliferation and differentiation in liver tissue[20,21]. Like Crol (Fig.S1), ZNF267 shows wide-ranged expression across human intestinal cell types (GTEx, Proteinatlas) and is induced through oestrogen signalling[22], which prompted us to investigate how steroid hormones control ISC proliferation downstream of Crol and ZNF267.

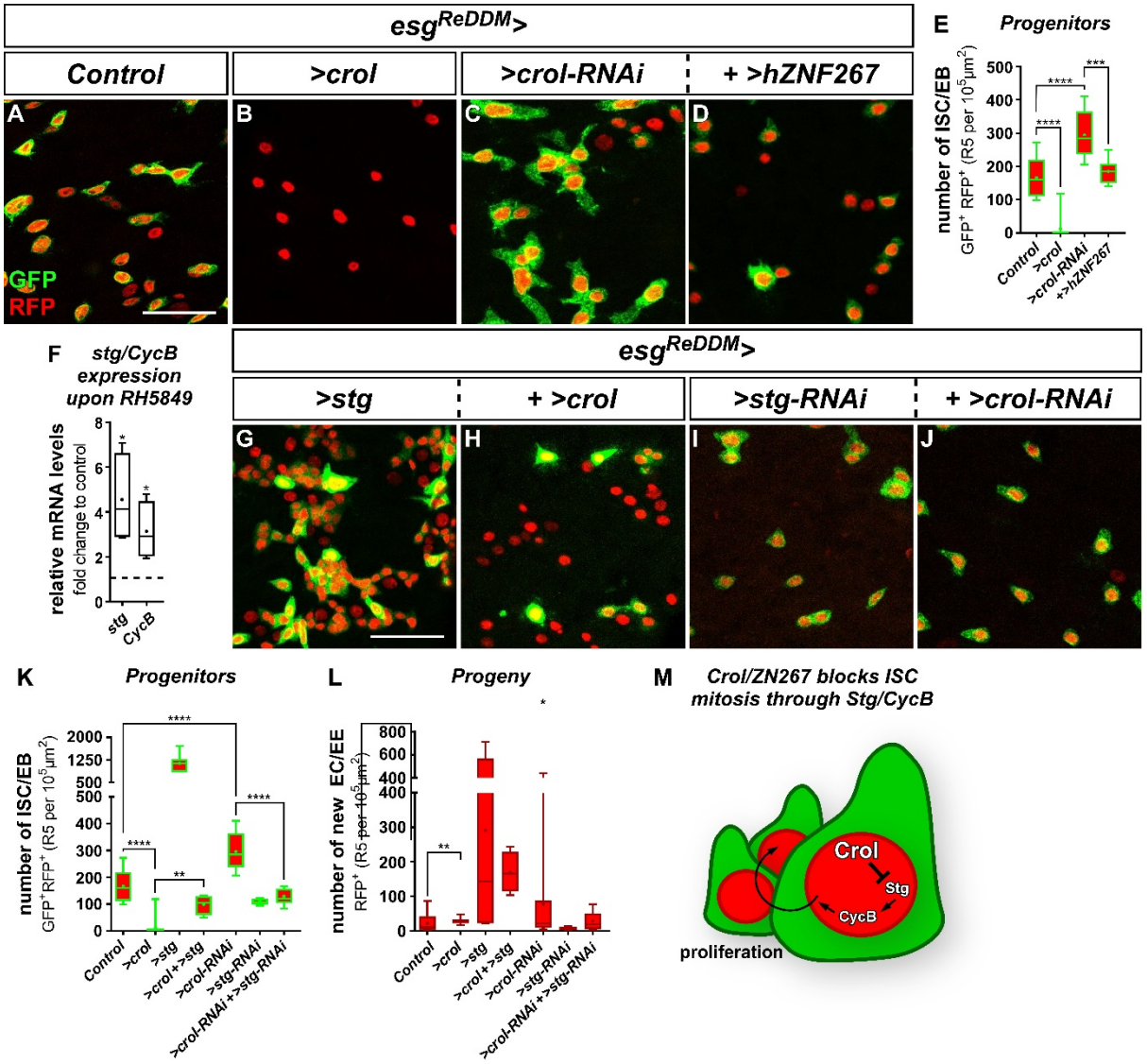

Fig.2: Crol and ZNF267 control ISC proliferation through String/Cyclin B

(A-C) Confocal images of adult female midguts after seven days of *esg*^{ReDDM} tracing showing (A) controls with active *esg-Gal4* in ISC/EB driving expression of *UAS-CD8::GFP* (membrane GFP) and *UAS-H2B::RFP* (nuclear RFP), and newly differentiated epithelial cells with inactive *esg-Gal4* are RFP+-only owing to protein stability of H2B::RFP, (B) ISC/EB specific overexpression (OE) of *UAS-crol* (UAS abbreviated as '>' hereafter in figure panels), (C) knockdown (KD) of *crol* by *>crol-RNAi*, and (D) simultaneous expression of the human Crol orthologue ZNF267 (*>hZNF267*). Scale bar is 50µm. (E) Quantification of progenitor cell numbers encompassing ISC and EB (n=9,10,15,12). Mean is indicated by (+) and asterisks denote significances from student's t-test (***p<0.001, ****p<0.0001). (F) Quantitative RT-PCR on intestinal cDNA from MF fed with 20HE agonist RH5849 showing relative mRNA levels of *string* (*stg*) and *Cyclin B* (*CycB*) (n=4,4). Values are normalized to MeOH control. (G-J) Confocal images of adult female midguts after seven days of *esg*^{ReDDM} tracing showing (G) ISC/EB specific OE of *stg* (H) combined with *>crol*, and (I) specific KD of *stg* by RNAi, (J) combined with *>crol-RNAi*. Scale bar is 50µm. (K-L) Quantifications of (K) progenitor cell numbers and (L) progeny (n=9,10,7,4,15,5,9/9,10,7,4,15,5,9). Mean is indicated by (+) and asterisks denote significances from student's t-test (*p<0.05, **p<0.01, ****p<0.0001). (L) Schematic showing inhibition of Stg and CycB by Crol within ISC thereby controlling proliferation.

Crol controls ISC proliferation through String and Cyclin B

During *Drosophila* development, it was shown that the tyrosine protein phosphatase *string* (*stg*, CDC25-orthologue) and the mitotic B-type Cyclin *CycB* are targets of EcR activity[23,24]. Supporting the idea that EcR-signalling controls ISC proliferation through Stg and CycB, EcR agonists not only increase ISC mitosis[4,8], but also *stg* and *CycB* transcript levels (Fig.2F). In line with previous observations[25,26], up- and downregulation of *stg* levels in *esg*^{ReDDM} traced guts

(Fig.2G,2I) reciprocally controlled progenitor (Fig.2K) and epithelial cell production (Fig.2L). Confirming a function of Stg downstream of EcR-signalling, ISC proliferation and subsequent increase in progenitor number upon *>crol-RNAi* is abolished when *>stg-RNAi* is co-expressed (Fig.2I-L,Fig.S3A) and *vice versa*, co-expression of *>crol* and *>stg* (Fig.2G-H) sufficed to rescue progenitor number (Fig.2K) and new EC production (Fig.2L). Comparable results were obtained when we investigated the epistasis of Crol and CycB (Fig.S3B-G), suggesting an endocrine control of ISC cell cycle exit by Crol (Fig.2M) as observed in development[24].

An anti-proliferative role of Crol in ISC is further supported by high Crol::GFP levels in EB (Fig.S3H) that become postmitotic during lineage progression[27]. As genetically shown for Crol and CycB (Fig.S3)[24], the EB lineage-specifying transcription factor *klumpfuss (klu)* binds CycB regulatory regions[27]. Pointing to a role in ISC, EB-lineage specific *crol* manipulation using klu^{ReDDM} (Fig.S3I)[28] reveals an increase in number of new EC upon forced expression of crol (Fig.S3J-L,N), but no significant changes on EB numbers (Fig.S3J-M), even though mitotic pH3-positive EB are occasionally observed upon *crol-RNAi* (Fig.S3O) and *CycB* expression (Fig.S3P). Together, our data highlights *crooked legs* as effector of Ecdysone-signalling that autonomously promotes ISC cell cycle exit through *stg* and *CycB* (Fig.2M).

The 20HE-Crol-Wg axis in Enterocytes controls non-autonomous Wnt/wg activity in intestinal stem cells

Intriguingly, *ZNF267*[20,21] as well as *crol*[24] connect steroid hormone and Wnt/wg-signalling, which prompted us to investigate whether Crol controls Wnt/wg-expression downstream of systemic 20HE-signalling during physiological mating-induced intestinal adaptations. Using transgenic flies in which Wg, the primary Wnt-ligand in *Drosophila*, is GFP-tagged (Wg::GFP), we detected GFP signal in EC anterior to the mid-/hindgut boundary (MHB, Fig.3A)[29], a gut region known to be patterned by Wnt/Wg-signalling[30]. Secreted Wg is thought to act in a paracrine manner on ISC, which we analysed using the established *frizzled3* (*fz3)* sensor flies for Wnt-activity (Fig.3K)[31,32]. Examining *fz3-RFP* intensity in posterior midguts, we confirmed an active Wnt-signalling crescendo towards the MHB[32]. More importantly, we detected fz3-RFP signal in intestinal progenitors along the midgut (Fig.3E) and occasional Wg::GFP positive EC close to ISC with fz3-activity (Fig.S4A) under homeostatic conditions.

Similar to 20HE-induced Crol::GFP (Fig.1A-C'',E), the EcR agonist RH5849 and *ovoD1* increased Wg::GFP fluorescence in EC (Fig.3A-D,I-J) and Wnt/Wg-activity in ISC/EB (Fig.3E-J), suggestive for active Wnt/Wg-signalling from EC to ISC (Fig.3K). Mating also increased Wg::GFP and fz3-RFP levels (Fig.S4B-F), which further supports a role of Wnt/wg-signalling during physiological midgut adaptations. Previous work in challenged guts showed autocrine Wnt/Wg-signalling between ISC and EB[33]. In contrast, depletion of wg using *>wg-RNAi* driven in esg^{ReDDM} flies under homeostatic conditions[28] did not significantly alter intestinal turnover (Fig.S5A-E) and direct assessment of Wnt/wg signalling activity using *fz3-RFP* sensor flies (Fig.S5F-I). Together these findings prompted us to search for another source for Wg-ligands under homeostatic conditions.

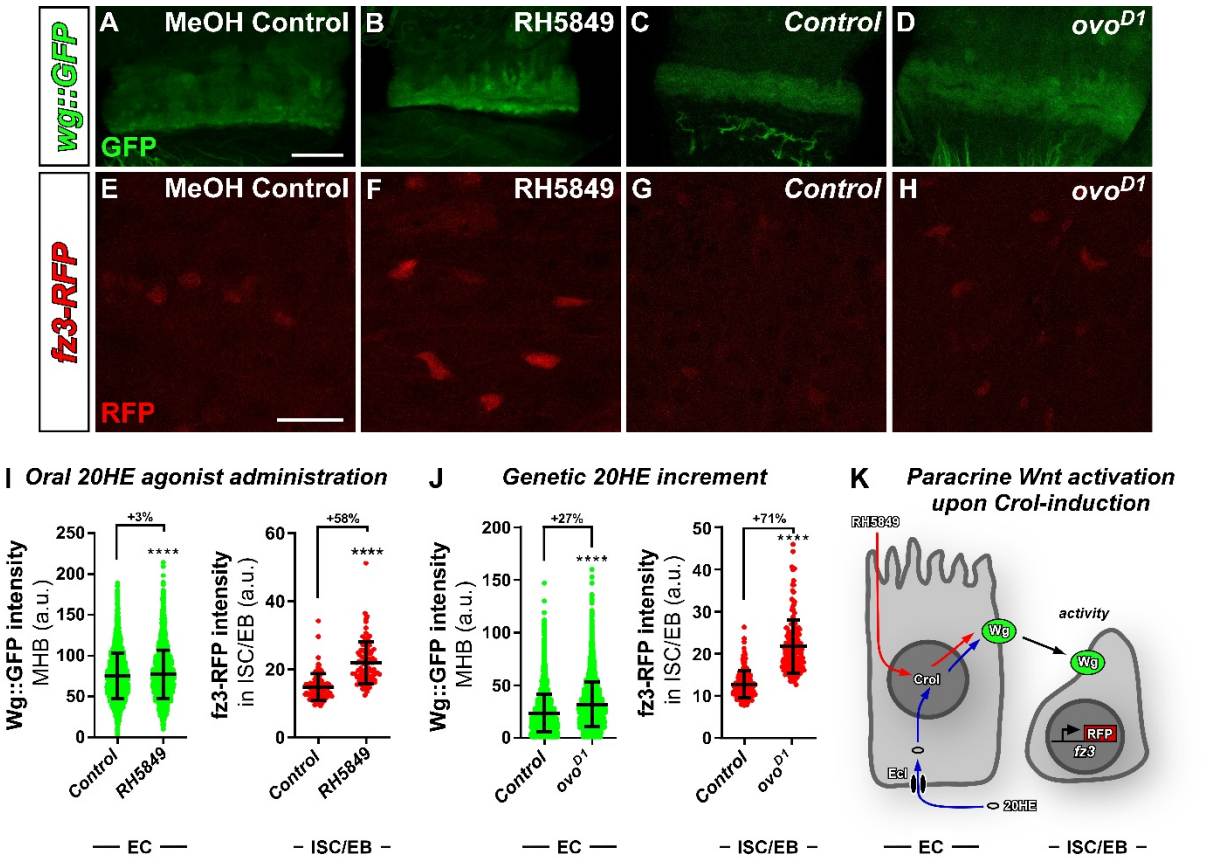

Fig.3: 20HE induced wg ligands from EC activate Wnt/wg signalling in ISC

(A-D) Confocal images of GFP-tagged Wnt ligand wingless (*wg::GFP*) in adult midguts of (A) MF fed with MeOH (MeOH Control) compared to (B) MF fed with 20HE agonist RH5849, and (C) control flies compared to heterozygous ovo^{D1} mutant MF. Scale bar is 50µm. (E-H) Confocal images of adult midguts with RFP expressed under control of the fz3 promotor (*fz3-RFP*) as readout for Wnt activity in (E) controls compared to (F) flies fed with RH5849, and (G) controls compared to (H) heterozygous ovo^{D1} mutant flies. Scale bar is 20µm. (I-J) Quantifications of Wg::GFP intensities in EC and fz3-RFP intensities in ISC/EB upon (I) oral administration of 20HE agonist RH5849 and (J) genetic 20HE increment upon ablation of ovaries. Fold changes are shown in percentages, means and standard deviations are indicated by vertical lines (n=7595,5192/90,90/8646,10874/178,168). Asterisks denote significances from student's t-test (****p<0.0001). (K) Schematic of paracrine Wnt/wg activation upon 20HE increment. RH5849 is incorporated into EC from the midgut lumen, whereas 20HE from surrounding hemolymph is imported into EC by the ecdysone importer (Ecl). Within EC the hormone or its agonist activate expression of *crol*, and expression of *wg*. Wg ligand is then secreted by the EC and non-autonomously activates Wnt/Wg signalling in ISC visible by expression of fz3-RFP.

Given Crol::GFP (Fig.S1C-C'') and Wg::GFP (Fig.S4A) signal in EC, we examined whether *wg* expression is controlled by 20HE and Crol in EC. Therefore, we combined the established EC-driver (*mex>*)[34] with *fz3-RFP* to enable Wnt-activity assessment in ISC/EB from non-autonomous sources (Fig.4A). In line with the idea of a 20HE-Crol-Wg axis, we found that increasing 20HE signalling pathway activity by EC-specific expression of *Ecl* (*Ecdysone importer*)[8,35], *crol* as well as *wg* significantly increased *fz3* activity in adjacent ISC/EB (Fig.4B, Fig.S5J-L',N-N'). Reciprocally, depletion of *Ecl*, *crol* and *wg* in EC, non-autonomously reduced *fz3* activity measured in ISC/EB (Fig.4B, Fig.S5O-P',R-R'). Consequently, Wg-depletion downstream of forced *crol* expression reduced paracrine fz3-activity measured in ISC/EB (Fig.4C,Fig.S5M-M'), whereas *ZNF267* expression in endogenous crol-depleted EC (Fig.4D, Fig.S5Q-Q') stimulated *wg* expression, further supporting Crol and its human orthologue ZNF267 acting on the *wg* expression control [14,24].

Combined, these findings suggest *wg* as a central transcriptional target of Crol in EC that non-autonomously stimulates fz3-activity in ISC. Intrigued by these observations, we investigated whether Wnt/Wg activation in epithelial EC through

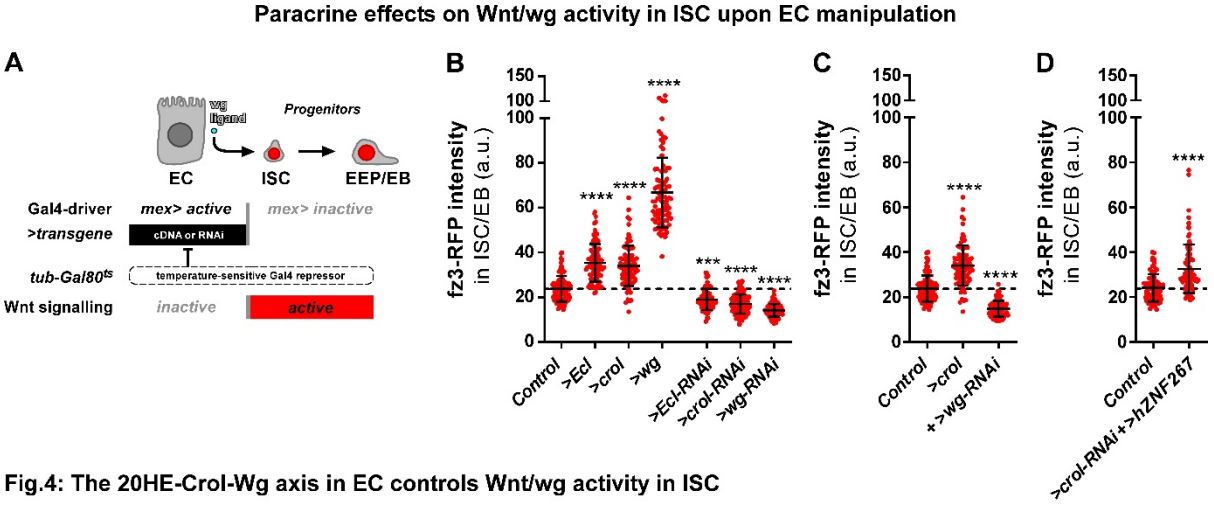

Fig.4: The 20HE-Crol-Wg axis in EC controls Wnt/wg activity in ISC

(A) Schematic of a system enabling EC manipulation and simultaneous visualization of Wnt/Wg activity in ISC/EB. *mex-Gal4* is active in EC and allows specific manipulation of EC by crossing to UAS-driven transgenes. These manipulations are timely controlled by an ubiquitously expressed temperature sensitive Gal4 repressor (*tub-Gal80^{ts}*) and combined with *fz3-RFP* sensor reflecting Wnt/Wg activity in ISC/EB independent of Gal4. (B-D) Quantifications of fz3-RFP intensities in ISC/EB with (B) OE and KD of *Ecl*, *crol* and *wg* (n=90,90,90,90,75,60,120), (C) EC specific OE of *crol* combined with *>wg-RNAi* (n=90,90,90), and (D) ectopic expression of *>hZNF267* in *crol* depleted EC (n=90,89). Means and standard deviations are indicated by vertical lines and asterisks denote significances from student's t-test (***p<0.001, ****p<0.0001).

the 20HE-Crol-Wg axis translates into stem cell driven intestinal homeostasis and size adaptation[4,7,8].

'Rapport' tracing reveals non-autonomous control of intestinal homeostasis through 20HE-Crol-Wg

For the investigation of paracrine effects on stem cell behaviour, we developed 'Rapport' ('Repressible activity paracrine reporter'), a dual binary expression system that combines spatiotemporally controlled transgene expression with ReDDM tracing of stem cell progeny. To preserve advantage of the existing established Gal4/UAS drivers and toolbox, we created an entirely new and Gal4-independent lexA/Aop-based '*esg^{lexReDDM}*' (*esg>>CD8::GFP, >>H2B::RFP, tub-Gal80^{ts}*) tracing system. Importantly, when combined with *mex-Gal4* (*mex>*) for EC specific expression[34], the lexA-operator driven in *esg^{lexReDDM}* as well as Gal4 driven by *mex* are repressed by temperature-sensitive Gal80^{ts}, which allows simultaneous temporally controlled onset of UAS-transgenes as well as *esg^{lexReDDM}* tracing and Aop-transgenes (Fig.5A)[36].

We confirmed Rapport tracing functionality by tracing outcrossed controls over three weeks (Fig.S6A-C) and observed an expected linear increase in intestinal renewal (Fig.S6E), while ISC/EB numbers remained constant (Fig.S6D)[19]. Previous reports described autocrine EGFR-stimulation resulting in ISC proliferation[25], which we confirmed by crossing Rapport to flies expressing the EGF ligand *Spitz* (*>spi*, TGF alpha homologue, Fig.S6F)[37].

Next, we assessed whether 20HE and Crol controlled Wnt/wg activity (Fig.4) stimulates ISC division resulting in EC production and organ size adaptation

(Fig.5A). Strikingly, forced expression of *Ecl, crol* and *wg* (Fig.5C-F) non-autonomously increased progenitor cell number (Fig.5J) and ISC progeny (Fig.5K) compared to controls (Fig.5B) when midguts were traced with Rapport. Reciprocally, depletion of *Ecl, crol* and *wg* reduced progenitor (Fig.5G-J) and progeny cell numbers (Fig.5K). These data reveal direct relay of 20HE activity in enterocytes into stem cell production mediated by Crol and paracrine Wnt/Wg-signal.

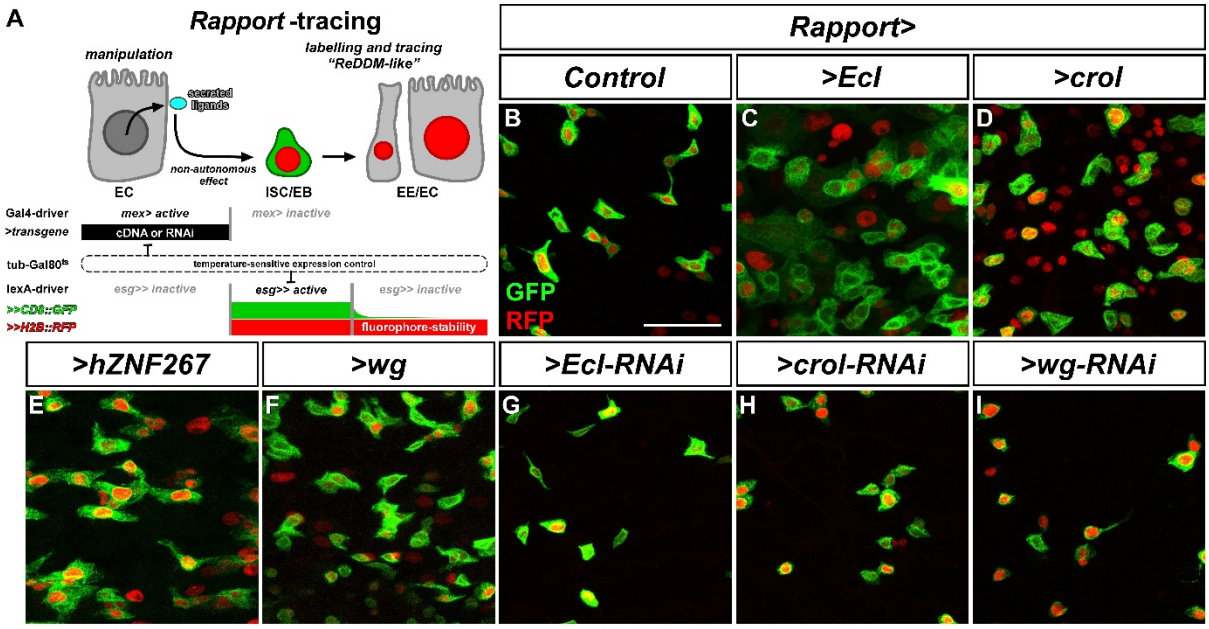

Fig.5: The 20HE-Crol-Wg axis in EC controls intestinal homeostasis

(A) Schematic of the newly developed 'Repressible activity paracrine reporter' (Rapport) tracing system. Rapport consist of a *mex-Gal4* driver enabling EC specific expression of UAS-driven cDNAs or RNAi constructs and an *esg^{lexReDDM}* system based on lexA/Aop allowing Gal4/UAS independent labelling and tracing of ISC/EB by *esg-lexA* driven expression of *Aop-CD8::GFP* and *Aop-H2B::mCherry* (lexA/Aop abbreviated as '>>' hereafter), both expression systems are timely controlled by a *tub-Gal80^{ts}* repressor. (B-I) Confocal images of adult midguts after (B,D-E,G-H) seven days or (C,F,I) 10 days of Rapport tracing of (B) controls, OE of (C) *Ecl*, (D) *crol*, (E) *hZNF267* and (F) *wg*, and KD of (G) *Ecl*, (H) *crol* and (I) *wg* showing GFP$^+$ and RFP$^+$ ISC/EB and their differentiated progeny labelled only by RFP. Scale bar is 50µm. (J-K) Quantifications of (J) progenitor cell numbers and (K) their progeny upon EC specific manipulations of *Ecl*, *crol*, *hZNF267* and *wg* (n=9,5,10,9,10,7,13,5/9,5,10,9,10,7,13,5). Mean is indicated by (+) and asterisks denote significances from student's t-test (*p<0.05, **p<0.01, ***p<0.001, ****p<0.0001).

The 20HE-Crol-Wg mitotic balance is conserved in intestinal tumours

Wnt-signalling is a well-known driver of tumorigenesis with a key role in cancers of the intestine. ZNF267 is upregulated in colorectal cancer (CRC) and regulates cell proliferation and differentiation in epithelial cancer entities[20,21]. We found that ZNF267 expression levels positively and negatively correlate with members of the Wnt-signalling pathway (Fig.S7A). CRC originates from ISC[38], which prompted us to investigate *crol* and ZNF267 in two established intestinal tumour models.

Investigating the autonomous role of Crol/ZNF267 in N loss-of-function (LOF, Fig.S7B) tumours[25,39-41] showed that forced expression of *crol* and ZNF267 within ISC reduced tumour number (Fig.6A-E) further underlining an anti-proliferative function in ISC. Growing evidence proves that microenvironmental Wnt/wg-ligands are an important contributor to the multifaceted process of colorectal tumorigenesis[42-46]. We thus extended Rapport with ISC-specific N-LOF that renders ISC incapable of EC lineage production and instead accumulate ISC- and EEP-like tumoral cells[25,39-41] (Fig.S7C). When we investigated Crol/ZNF267 in EC, we found that >*crol* boosts ISC tumour cell mass by 4-fold leading to confluent tumours

along the midgut (Fig.6F-J) comparable to tumour-induction by microenvironmentally-derived mitogenic EGF ligands[37,47].

Even though Notch-tumours recapitulate important steps of CRC tumorigenesis, N is not frequently mutated in CRC. Therefore, we also investigated an autonomous

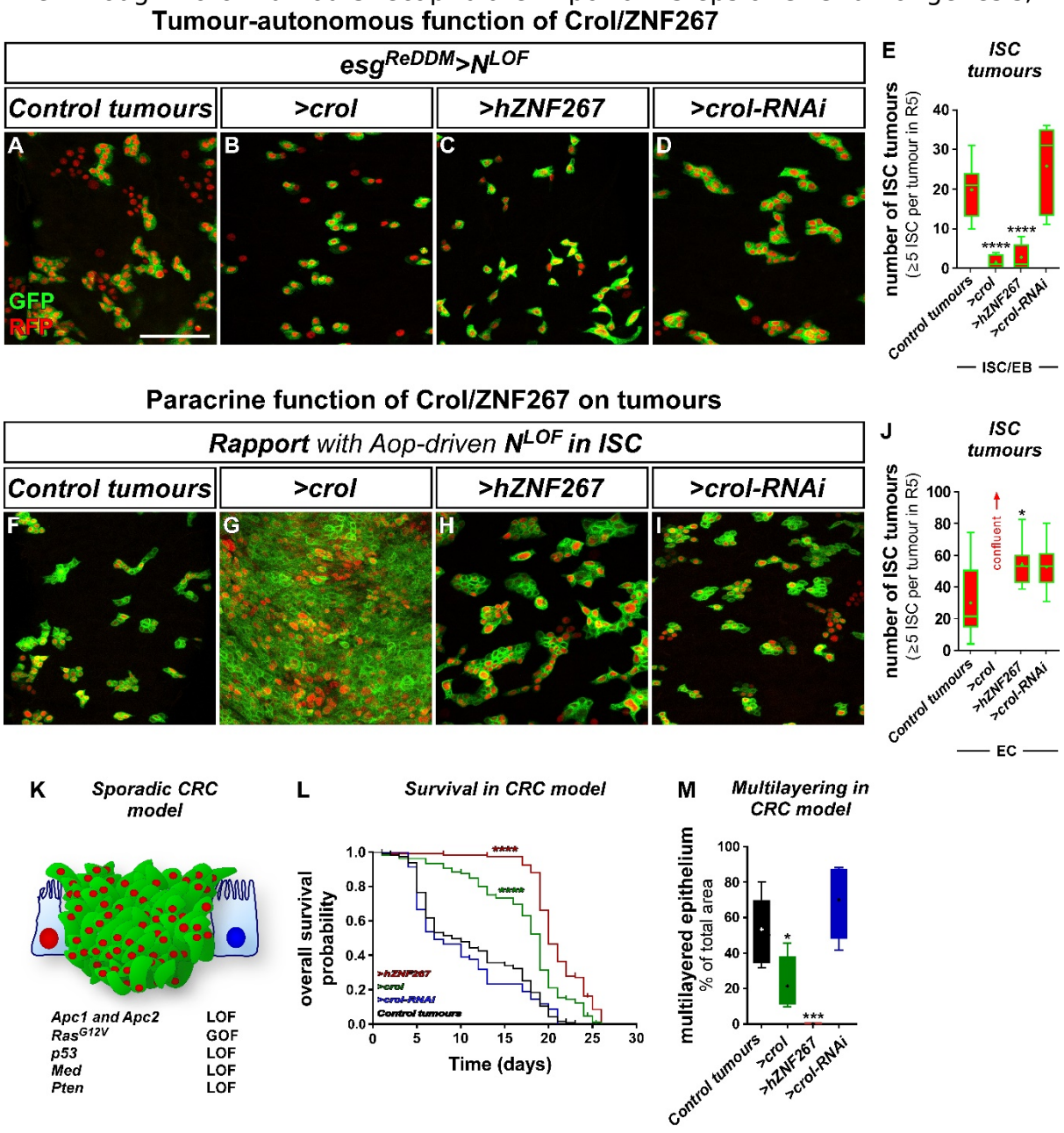

Fig.6: The mitotic balance of Crol/ZNF267 is preserved in intestinal tumour models

(A-D) Confocal images of adult midguts with ISC specific Notch loss of function (N^{LOF}) combined with esg^{ReDDM} tracing after three days of shifting in (A) controls, combined with (B) OE of *crol*, (C) expression of *>hZNF267*, and (D) *>crol-RNAi*. Scale bar is 50µm. (E) Quantification of ISC tumours encompassing number of clusters with 5 or more ISC (n=11,8,8,10). Mean is indicated by (+) and asterisks denote significances from student's t-test (****p<0.0001). (F-I) Confocal images of adult midguts with ISC specific N^{LOF} by expression of *Aop-N-RNAi* under control of *esg-lexA* within the Rapport tracing system after seven days of tracing in (F) controls, combined with EC specific (G) OE of *crol*, (H) expression of *>hZNF267*, and (I) *>crol-RNAi*. (J) Quantification of ISC tumours combined with EC specific manipulations of *crol*/*hZNF267* (n=10,-,10,10). Mean is indicated by (+) and asterisks denote significances from student's t-test (*p<0.05). (K) Schematic of a *Drosophila* CRC model combined with esg^{ReDDM} inducing formation of malignant tumours by ISC/EB specific expression of oncogenic *RasG12V* (gain of function, GOF) and CRISPR/Cas9 induced KO of *Apc1, Apc2, p53, Med,* and *Pten* (loss of function, LOF). (L) Kaplan-Meier estimation of survival in CRC model combined with manipulations of *crol*/*hZNF267* (n=119,121,118,69). Asterisks denote significances from Kaplan-Meier analysis (****p<0.0001). (M) Quantification of multilayered tissue encompassing percentage of area with intact EC indicated by anti-Dlg1 staining (n=7,4,4,7). Mean is indicated by (+) and asterisks denote significances from student's t-test (*p<0.05, ***p<0.001).

function for Crol/ZNF267 in a CRISPR-Cas9 based model of sporadic CRC[48] targeting the most frequently mutated genes with a multiplex guideRNA array (Fig.6K)[48-50]. CRC in ISC has severe and pleiotropic cellular phenotypes and results in early fly demise[48]. Underlining the antiproliferative autonomous role of *crol* and ZNF267, their forced expression significantly improved fly survival (Fig.S6L) as well as midgut length as a readout for epithelial hypotrophy and deterioration (Fig.6M)[8]. An established measure for epithelial integrity in intestinal tumour models is multilayering of epithelial cells[50-52], which is significantly reduced in tumoral midguts expressing *>crol* and *>ZNF267* (Fig.S7D).

These functional experiments in colorectal tumour paradigms additionally support the idea of a mitotic balance controlling intestinal growth. Overall, steroidal input on Crol in ISC (Fig.2) and EC (Fig.5) provides evidence for an endocrine intestinal size control implicated in mating hyperplasia. Indeed, mitogenic *crol*-depletion in ISC with esg^{ReDDM} increases the size of the mating-responsive R5 posterior midgut region (Fig.7A-A')[7], whereas forced *crol* expression in EC using Rapport elicits R5 growth (Fig.7B-B'). Finally, we tested our hypothesis of hormonally controlled intestinal size in a mathematical model.

Mathematical modelling of endocrine relay by Crol in the control of ISC proliferation underlines complex hormonal actions on intestinal size adaptation

Our model tests whether it is mathematically plausible that these opposing trends between mitotic and antiproliferative stimuli based on the molecular mechanisms found in this study induce stable population sizes that change consistently with 20HE levels. Assuming constant 20HE levels in VF and a higher constant 20HE level in MF[8], we tested the hypothesis whether an 20HE increment is capable to yield a stable, larger organ by temporarily boosting ISC mitosis (Fig.7D), which then declines through the increment of EC numbers and their anti-proliferative effect on ISC mitosis.

Constant hormonal input produces equal amounts of mitogenic Wnt/Wg independent of EC numbers. As a logical consequence of the increase in EC numbers[7,8] and constant ISC numbers (Fig.S7E), the average EC to ISC distance increases (Fig.7C-C'). In consequence, the amount of Wnt/Wg produced in the direct neighbourhood of an ISC decays with the increase of EC[53]. Considering a section of the intestine as a 1D ring, the exponential functional shape of the decay of morphogen gradient described in detail for Wg[54](see supplementary material) holds. Therefore, the average amount of mitogenic Wnt/wg-ligand reaching equidistantly scattered ISC[39,41] will decline sharply when intestinal size increases (Fig.7C-C'). Thus, only the close EC neighbourhood of the ISC effectively contributes to the Wnt/Wg levels playing an active role in ISC proliferation. Consequently, in the equation of evolution for the number of EC, we have a mitotic term that is proportional to the concentration of 20HE —and, consequently, inverse to the number of EC — and an anti-proliferative term that can be assumed to be constant or, in a more general setting, declining slower than the mitotic term as a function of the concentration. Overall, the equation of evolution for the number of EC reads:

$$\frac{\Delta E}{\Delta t} = \beta C \frac{\gamma}{E} I - \alpha I$$

where E is the number of EC, C is a constant reproducing the effect of the neighbourhood, $\gamma(t)$ the net amount of hormone, I the number of ISC cells and α the anti-proliferative rate (Fig.7E). Qualitatively, the key result is that the above equation has a stable, fixed point for the amount of EC that grows and declines depending on whether the net amount of 20HE hormone grows or declines

(Fig.7F). We provide detailed information about the construction and mathematical properties of the model in the supplementary information[55,56].

In a second modelling approach, we hypothetically explored how constant EC numbers as generated in N-LOF tumours intestines would affect ISC division dynamics (Fig.S7B,F). With constant EC numbers and hormone level (Fig.7D), ISC counts in our model increase in a square-root-like manner (Fig.S7H) as the ISC population provides a growing sink for Wg. *In vivo,* block of EC generation and organ size is recapitulated in N-LOF tumours using Rapport (Fig.6F), where upregulation of Crol/ZNF267 dramatically increases ISC numbers (Fig.6J). Our discovered interdependencies between cell population sizes, Wnt/wg-degradation and their endocrine mitotic balance shed light on the complex endocrine involvement when tumour growth mechanisms are investigated. Together, our model is capable of capturing the emergence of a stable organ size from the antagonism of mitogenic and anti-proliferative hormonal input on ISC thresholding organ size as suggested by our functional data.

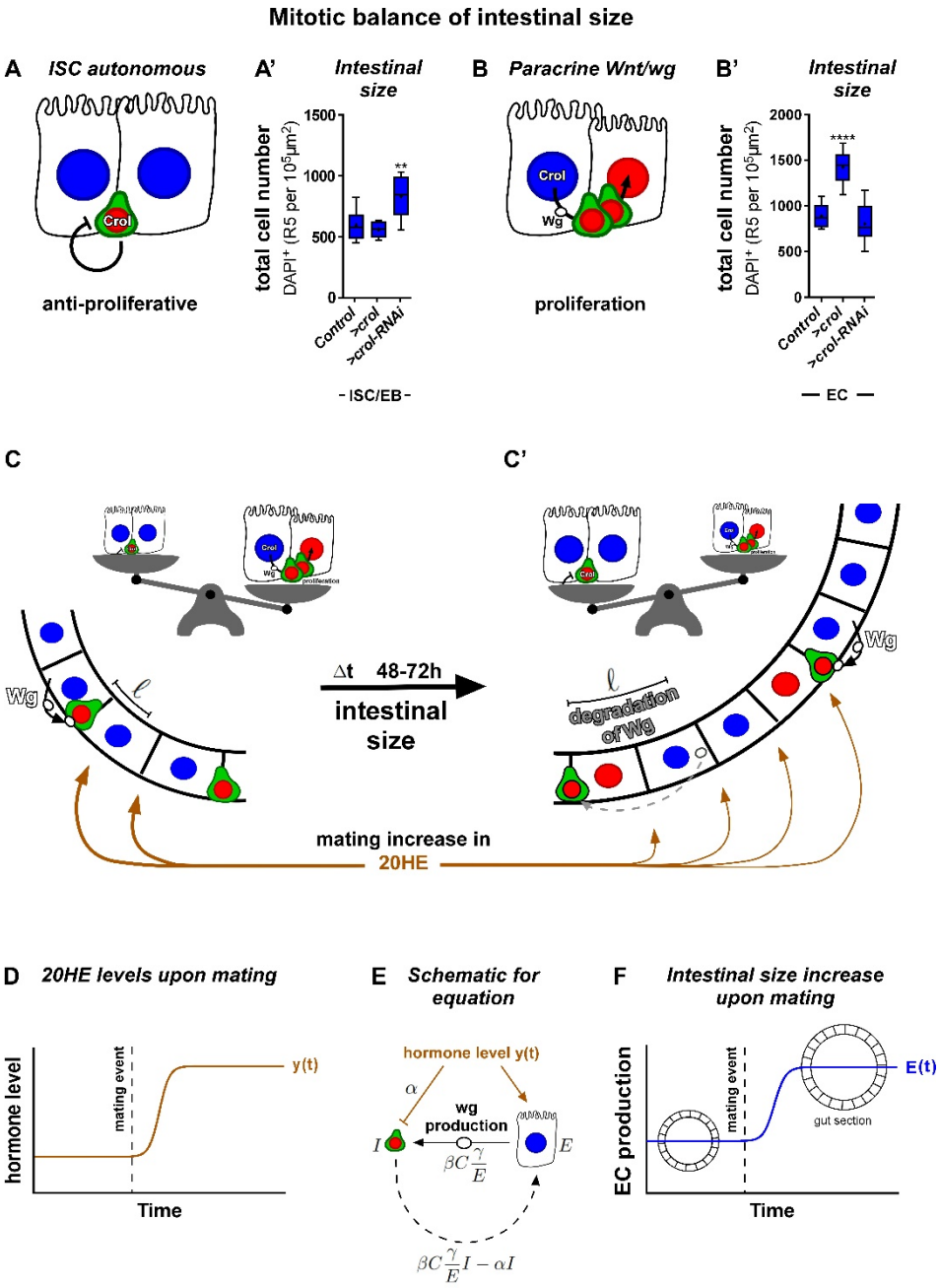

Fig.7: Mathematical modelling of hormone level controlled intestinal size

(A) Schematic of ISC autonomous function of Crol inhibiting ISC proliferation. (A') Quantification of intestinal size encompassing total cell number upon ISC/EB specific manipulations of *crol* (n=13,8,8). (B) Schematic of paracrine Wnt/wg release in EC regulated by Crol and inducing ISC proliferation. (B') Quantification of intestinal size encompassing total cell number upon EC specific manipulations of crol (n=9,10,17). Mean is indicated by (+) and asterisks denote significances from student's t-test (**p<0.01), ****p<0.0001). (C) Schematic of a gut section showing EC that release Wg ligand upon mating increase in 20HE signalling. Secreted Wg reaches ISC with a distance of ℓ. In a growing organ the function of Crol in inducing proliferation dominates the anti-proliferative function. (C') Upon an increase in intestinal size within 48-72h resulting in increasing EC number and thereby an increase in the average distance ℓ of EC (Wg source) and the ligand receiving ISC. With a longer distance ℓ Wg ligand degrades leading to a decrease in Wg concentration sensed by ISC and thereby to a decline in ISC proliferation. (D) A graph showing 20HE levels upon mating as a function ($\gamma(t)$) of hormone level per time. (E) Schematic for equation visualizing the divergent effect of 20HE hormone on ISC (I) inhibiting ISC proliferation and on EC (E) stimulating Wg production $\beta C \frac{\gamma}{E}$. Secreted Wg ligand stimulates ISC (I) to produce more EC (E) $\beta C \frac{\gamma}{E} I - \alpha I$. (F) A graph visualizing intestinal size increase upon mating as a function ($E(t)$) of EC production per time with a growing gut section following the mating event indicating intestinal growth.

Discussion

Here we identify the transcription factor *crooked legs* as coordinator of endocrine input into intestinal organ size. The discovered molecular mechanisms underline the complexity of heterologous cellular interactions: a hormonal stimulus bifurcates on stem cells and microenvironment, where it is relayed differently into an antiproliferative and a mitogenic stimulus. This interdependent opposing crosstalk of forces balances stem cell divisions and ultimately stabilizes organ size, which is sustained by both, empirical observations and mathematical modelling.

Our novel Rapport system contributes to disentangle the underlying endocrine and local signalling organ size control mechanisms, by allowing precise genetic intervention in cell types surrounding the ISC. The independent tracing of the whole stem cell population and easy fluorophore identification of different fate choices ensures robust progeny counts in fluctuating demand situations compared to previous systems[25,37,47]. Endocrine actions on ISC are complex and involve hormonal dosage and mating status[4,7,8], sex differences[57] and feeding[58]. Hypertrophy upon pregnancy is described in the mammalian gut[1,3] and is well-studied in reproductive organs such as the mammary epithelium where steroid hormones induce dramatic remodelling and cancer susceptibility[59-61].

In gastrointestinal tumours such as CRC, epidemiological evidence about the role of steroid hormones remains controversial and ranges from favourable to detrimental[62-68]. Functional studies of both mammalian oestrogen receptors (ER) in rodents underline the complexity of oestrogen signalling in gut tumorgenicity[69,70] and reveal further complexities as pharmacological (E2/P4) and endogenous oestradiol levels differentially affect patient outcome[62,65,71]. Our functional and modelling data provides an initial logic to disentangle complex observations and involves the heterogeneity of tumour cell composition and its capacity to contribute to mitotic signals.

A targeted therapeutic intervention of steroid hormone signalling is supported by: i) an overall protective tendency of ER signalling in CRC[68]. ii) Like Crol, ZNF267 is stimulated by ER[22] and is involved in Wnt signalling[20,21] suggesting conservation of the 20HE-Crol-Wg axis. iii) Wnt/wg signalling hyperactivation is central to CRC malignancy and Wnt-ligands remain indispensable for CRC growth albeit absence of APC[72]. iv) Effectors of steroid signalling like PPARγ/Eip75B play protective roles in fly pathophysiology[4,8] and human disease[73,74].

Our findings of antagonizing autonomous and paracrine effects of Crol and ZNF267 on tumour growth (Fig.6G-K, Fig.S7) emphasize that targeted genetic investigation is of key importance to understand how mutational heterogeneity and cell type composition differentially affect the proliferative response to hormonal input. Precise intervention and tracing methods such as Rapport open the door for untangling heterogenous findings of epidemiological and functional studies.

3451 words

Bibliography

1. Hammond, K.A. Adaptation of the maternal intestine during lactation. *J Mammary Gland Biol Neoplasia* **2**, 243-52 (1997).
2. Roa, J. & Tena-Sempere, M. Connecting metabolism and reproduction: roles of central energy sensors and key molecular mediators. *Mol Cell Endocrinol* **397**, 4-14 (2014).
3. Speakman, J.R. The physiological costs of reproduction in small mammals. *Philosophical Transactions of the Royal Society B: Biological Sciences* **363**, 375-398 (2008).
4. Ahmed, S.M.H. *et al.* Fitness trade-offs incurred by ovary-to-gut steroid signalling in Drosophila. *Nature* **584**, 415-419 (2020).
5. Cognigni, P., Bailey, A.P. & Miguel-Aliaga, I. Enteric neurons and systemic signals couple nutritional and reproductive status with intestinal homeostasis. *Cell Metab* **13**, 92-104 (2011).
6. Klepsatel, P. *et al.* Reproductive and post-reproductive life history of wild-caught Drosophila melanogaster under laboratory conditions. *J Evol Biol* **26**, 1508-20 (2013).
7. Reiff, T. *et al.* Endocrine remodelling of the adult intestine sustains reproduction in Drosophila. *Elife* **4**, e06930 (2015).
8. Zipper, L., Jassmann, D., Burgmer, S., Gorlich, B. & Reiff, T. Ecdysone steroid hormone remote controls intestinal stem cell fate decisions via the PPARgamma-homolog Eip75B in Drosophila. *Elife* **9**, e55795 (2020).
9. Ameku, T. & Niwa, R. Mating-Induced Increase in Germline Stem Cells via the Neuroendocrine System in Female Drosophila. *PLoS Genet* **12**, e1006123 (2016).
10. Harshman, L.G., Loeb, A.M. & Johnson, B.A. Ecdysteroid titers in mated and unmated Drosophila melanogaster females. *J Insect Physiol* **45**, 571-577 (1999).
11. Lin, G., Xu, N. & Xi, R. Paracrine Wingless signalling controls self-renewal of Drosophila intestinal stem cells. *Nature* **455**, 1119-23 (2008).
12. Radtke, F. & Clevers, H. Self-renewal and cancer of the gut: two sides of a coin. *Science* **307**, 1904-9 (2005).
13. D'Avino, P.P. & Thummel, C.S. crooked legs encodes a family of zinc finger proteins required for leg morphogenesis and ecdysone-regulated gene expression during Drosophila metamorphosis. *Development* **125**, 1733-45 (1998).
14. Mitchell, N., Cranna, N., Richardson, H. & Quinn, L. The Ecdysone-inducible zinc-finger transcription factor Crol regulates Wg transcription and cell cycle progression in Drosophila. *Development* **135**, 2707-16 (2008).
15. Mitchell, K.J. *et al.* Genetic analysis of Netrin genes in Drosophila: Netrins guide CNS commissural axons and peripheral motor axons. *Neuron* **17**, 203-15 (1996).
16. Dutta, D. *et al.* Regional Cell-Specific Transcriptome Mapping Reveals Regulatory Complexity in the Adult Drosophila Midgut. *Cell Rep* **12**, 346-58 (2015).
17. Hung, R.J., Li, J.S.S., Liu, Y. & Perrimon, N. Defining cell types and lineage in the Drosophila midgut using single cell transcriptomics. *Curr Opin Insect Sci* **47**, 12-17 (2021).
18. Busson, D., Gans, M., Komitopoulou, K. & Masson, M. Genetic Analysis of Three Dominant Female-Sterile Mutations Located on the X Chromosome of DROSOPHILA MELANOGASTER. *Genetics* **105**, 309-25 (1983).

19. Antonello, Z.A., Reiff, T., Ballesta-Illan, E. & Dominguez, M. Robust intestinal homeostasis relies on cellular plasticity in enteroblasts mediated by miR-8-Escargot switch. *EMBO J* **34**, 2025-41 (2015).
20. Schnabl, B., Valletta, D., Kirovski, G. & Hellerbrand, C. Zinc finger protein 267 is up-regulated in hepatocellular carcinoma and promotes tumor cell proliferation and migration. *Exp Mol Pathol* **91**, 695-701 (2011).
21. Yang, H. *et al.* Knockdown of zinc finger protein 267 suppresses diffuse large B-cell lymphoma progression, metastasis, and cancer stem cell properties. *Bioengineered* **13**, 1686-1701 (2022).
22. Stossi, F. *et al.* Transcriptional profiling of estrogen-regulated gene expression via estrogen receptor (ER) alpha or ERbeta in human osteosarcoma cells: distinct and common target genes for these receptors. *Endocrinology* **145**, 3473-86 (2004).
23. Li, T.R. & White, K.P. Tissue-specific gene expression and ecdysone-regulated genomic networks in Drosophila. *Dev Cell* **5**, 59-72 (2003).
24. Mitchell, N.C. *et al.* The Ecdysone receptor constrains wingless expression to pattern cell cycle across the Drosophila wing margin in a Cyclin B-dependent manner. *BMC Dev Biol* **13**, 28 (2013).
25. Patel, P.H., Dutta, D. & Edgar, B.A. Niche appropriation by Drosophila intestinal stem cell tumours. *Nat Cell Biol* **17**, 1182-92 (2015).
26. Zhang, P. *et al.* An SH3PX1-Dependent Endocytosis-Autophagy Network Restrains Intestinal Stem Cell Proliferation by Counteracting EGFR-ERK Signaling. *Dev Cell* **49**, 574-589 e5 (2019).
27. Korzelius, J. *et al.* The WT1-like transcription factor Klumpfuss maintains lineage commitment of enterocyte progenitors in the Drosophila intestine. *Nat Commun* **10**, 4123 (2019).
28. Reiff, T. *et al.* Notch and EGFR regulate apoptosis in progenitor cells to ensure gut homeostasis in Drosophila. *EMBO J* **38**, e101346 (2019).
29. Port, F., Chen, H.M., Lee, T. & Bullock, S.L. Optimized CRISPR/Cas tools for efficient germline and somatic genome engineering in Drosophila. *Proc Natl Acad Sci U S A* **111**, E2967-76 (2014).
30. Takashima, S., Mkrtchyan, M., Younossi-Hartenstein, A., Merriam, J.R. & Hartenstein, V. The behaviour of Drosophila adult hindgut stem cells is controlled by Wnt and Hh signalling. *Nature* **454**, 651-5 (2008).
31. Olson, E.R. *et al.* Yan, an ETS-domain transcription factor, negatively modulates the Wingless pathway in the Drosophila eye. *EMBO reports* **12**, 1047-1054 (2011).
32. Tian, A. *et al.* Intestinal stem cell overproliferation resulting from inactivation of the APC tumor suppressor requires the transcription cofactors Earthbound and Erect wing. *PLoS Genet* **13**, e1006870 (2017).
33. Cordero, J.B., Stefanatos, R.K., Scopelliti, A., Vidal, M. & Sansom, O.J. Inducible progenitor-derived Wingless regulates adult midgut regeneration in Drosophila. *EMBO J* **31**, 3901-17 (2012).
34. Phillips, M.D. & Thomas, C.M. Brush border spectrin is required for early endosome recycling in Drosophila. *J Cell Sci* **119**, 1361-70 (2006).
35. Okamoto, N. *et al.* A Membrane Transporter Is Required for Steroid Hormone Uptake in Drosophila. *Dev Cell* **47**, 294-305 e7 (2018).
36. Yagi, R., Mayer, F. & Basler, K. Refined LexA transactivators and their use in combination with the Drosophila Gal4 system. *Proc Natl Acad Sci U S A* **107**, 16166-71 (2010).
37. Liang, J., Balachandra, S., Ngo, S. & O'Brien, L.E. Feedback regulation of steady-state epithelial turnover and organ size. *Nature* **548**, 588-591 (2017).

38. Barker, N. *et al.* Crypt stem cells as the cells-of-origin of intestinal cancer. *Nature* **457**, 608-11 (2009).
39. Micchelli, C.A. & Perrimon, N. Evidence that stem cells reside in the adult Drosophila midgut epithelium. *Nature* **439**, 475-9 (2006).
40. Ohlstein, B. & Spradling, A. Multipotent Drosophila intestinal stem cells specify daughter cell fates by differential notch signaling. *Science* **315**, 988-92 (2007).
41. Ohlstein, B. & Spradling, A. The adult Drosophila posterior midgut is maintained by pluripotent stem cells. *Nature* **439**, 470-4 (2006).
42. Vermeulen, L. *et al.* Wnt activity defines colon cancer stem cells and is regulated by the microenvironment. *Nat Cell Biol* **12**, 468-76 (2010).
43. Hanahan, D. & Weinberg, Robert A. Hallmarks of Cancer: The Next Generation. *Cell* **144**, 646-674 (2011).
44. Patel, S., Alam, A., Pant, R. & Chattopadhyay, S. Wnt Signaling and Its Significance Within the Tumor Microenvironment: Novel Therapeutic Insights. *Front Immunol* **10**, 2872 (2019).
45. McAllister, S.S. & Weinberg, R.A. The tumour-induced systemic environment as a critical regulator of cancer progression and metastasis. *Nat Cell Biol* **16**, 717-27 (2014).
46. Hanahan, D. Hallmarks of Cancer: New Dimensions. *Cancer Discovery* **12**, 31-46 (2022).
47. Ngo, S., Liang, J., Su, Y.H. & O'Brien, L.E. Disruption of EGF Feedback by Intestinal Tumors and Neighboring Cells in Drosophila. *Curr Biol* **30**, 1537-1546 e3 (2020).
48. Zipper, L., Batchu, S., Kaya, N.H., Antonello, Z.A. & Reiff, T. The MicroRNA miR-277 Controls Physiology and Pathology of the Adult Drosophila Midgut by Regulating the Expression of Fatty Acid beta-Oxidation-Related Genes in Intestinal Stem Cells. *Metabolites* **12**(2022).
49. Hanahan, D. & Weinberg, R.A. The hallmarks of cancer. *Cell* **100**, 57-70 (2000).
50. Bangi, E., Murgia, C., Teague, A.G., Sansom, O.J. & Cagan, R.L. Functional exploration of colorectal cancer genomes using Drosophila. *Nat Commun* **7**, 13615 (2016).
51. Martorell, O. *et al.* Conserved mechanisms of tumorigenesis in the Drosophila adult midgut. *PLoS One* **9**, e88413 (2014).
52. Zhai, Z. *et al.* Accumulation of differentiating intestinal stem cell progenies drives tumorigenesis. *Nature Communications* **6**, 10219 (2015).
53. Dubois, L., Lecourtois, M., Alexandre, C., Hirst, E. & Vincent, J.P. Regulated endocytic routing modulates wingless signaling in Drosophila embryos. *Cell* **105**, 613-24 (2001).
54. Dubois, L., Lecourtois, M., Alexandre, C., Hirst, E. & Vincent, J.-P. Regulated Endocytic Routing Modulates Wingless Signaling in Drosophila Embryos. *Cell* **105**, 613-624 (2001).
55. Wartlick, O., Kicheva, A. & González-Gaitán, M. Morphogen gradient formation. *Cold Spring Harb Perspect Biol* **1**, a001255 (2009).
56. Berg, H.C. *Random Walks in Biology*, (Princeton University Press, 1993).
57. Hudry, B., Khadayate, S. & Miguel-Aliaga, I. The sexual identity of adult intestinal stem cells controls organ size and plasticity. *Nature* **530**, 344-8 (2016).
58. O'Brien, L.E., Soliman, S.S., Li, X. & Bilder, D. Altered modes of stem cell division drive adaptive intestinal growth. *Cell* **147**, 603-14 (2011).
59. Joshi, P.A., Di Grappa, M.A. & Khokha, R. Active allies: hormones, stem cells and the niche in adult mammopoiesis. *Trends in Endocrinology & Metabolism* **23**, 299-309 (2012).

60. Russo, J. & Russo, I.H. The role of estrogen in the initiation of breast cancer. *J Steroid Biochem Mol Biol* **102**, 89-96 (2006).
61. Yager, J.D. & Davidson, N.E. Estrogen carcinogenesis in breast cancer. *N Engl J Med* **354**, 270-82 (2006).
62. Barzi, A., Lenz, A.M., Labonte, M.J. & Lenz, H.J. Molecular pathways: Estrogen pathway in colorectal cancer. *Clin Cancer Res* **19**, 5842-8 (2013).
63. Chlebowski, R.T. *et al.* Estrogen plus progestin and colorectal cancer in postmenopausal women. *N Engl J Med* **350**, 991-1004 (2004).
64. Foster, P.A. Oestrogen and colorectal cancer: mechanisms and controversies. *Int J Colorectal Dis* **28**, 737-49 (2013).
65. Manson, J.E. *et al.* Menopausal Hormone Therapy and Long-term All-Cause and Cause-Specific Mortality: The Women's Health Initiative Randomized Trials. *JAMA* **318**, 927-938 (2017).
66. Nie, X., Xie, R. & Tuo, B. Effects of Estrogen on the Gastrointestinal Tract. *Dig Dis Sci* **63**, 583-596 (2018).
67. Simon, M.S. *et al.* Estrogen plus progestin and colorectal cancer incidence and mortality. *J Clin Oncol* **30**, 3983-90 (2012).
68. Nakhostin, L., Stadler, A. & Stute, P. Impact of menopausal hormone therapy on colorectal cancer risk-A systematic review. *Clin Endocrinol (Oxf)* **95**, 390-397 (2021).
69. Campbell-Thompson, M., Lynch, I.J. & Bhardwaj, B. Expression of estrogen receptor (ER) subtypes and ERbeta isoforms in colon cancer. *Cancer Res* **61**, 632-40 (2001).
70. Hoff, M.B., Chang, W.W. & Mak, K.M. Effect of estrogen on cell proliferation in colonic mucosa of the mouse. *Virchows Arch B Cell Pathol Incl Mol Pathol* **35**, 263-73 (1981).
71. Charlton, B.M. *et al.* Oral contraceptive use and colorectal cancer in the Nurses' Health Study I and II. *Cancer Epidemiol Biomarkers Prev* **24**, 1214-21 (2015).
72. Voloshanenko, O. *et al.* Wnt secretion is required to maintain high levels of Wnt activity in colon cancer cells. *Nat Commun* **4**, 2610 (2013).
73. Lecarpentier, Y., Claes, V., Vallée, A. & Hébert, J.L. Interactions between PPAR Gamma and the Canonical Wnt/Beta-Catenin Pathway in Type 2 Diabetes and Colon Cancer. *PPAR Res* **2017**, 5879090 (2017).
74. Sabatino, L. *et al.* Emerging role of the beta-catenin-PPARgamma axis in the pathogenesis of colorectal cancer. *World J Gastroenterol* **20**, 7137-51 (2014).

Supplemental Figures

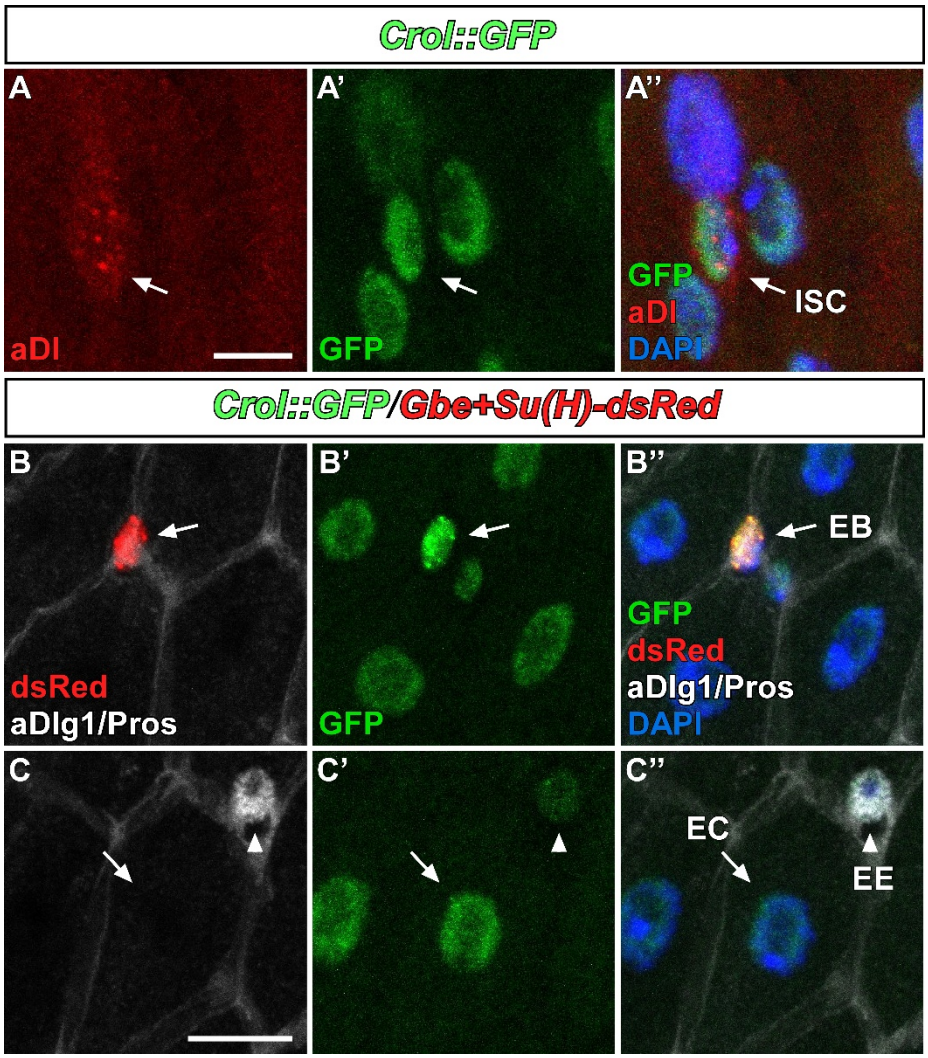

Fig.S1: Crol is expressed in the adult *Drosophila* midgut
(A-A'') Confocal images of Crol::GFP in adult midguts of MF showing localization of Crol in nuclei of ISC positive for antibody staining against the ISC marker Delta (aDl). Scale bar is 5µm. (B-C'') Confocal images of Crol::GFP combined with the EB marker Gbe+Su(H)-dsRed showing Crol localization in (B-B'') dsRed positive EC, and (C-C'') in epithelial EC stained with antibody against the septate junction marker discs large 1 (aDlg1) and enteroendocrine cells (EE) stained by anti-prospero (Pros). Scale bar is 10µm.

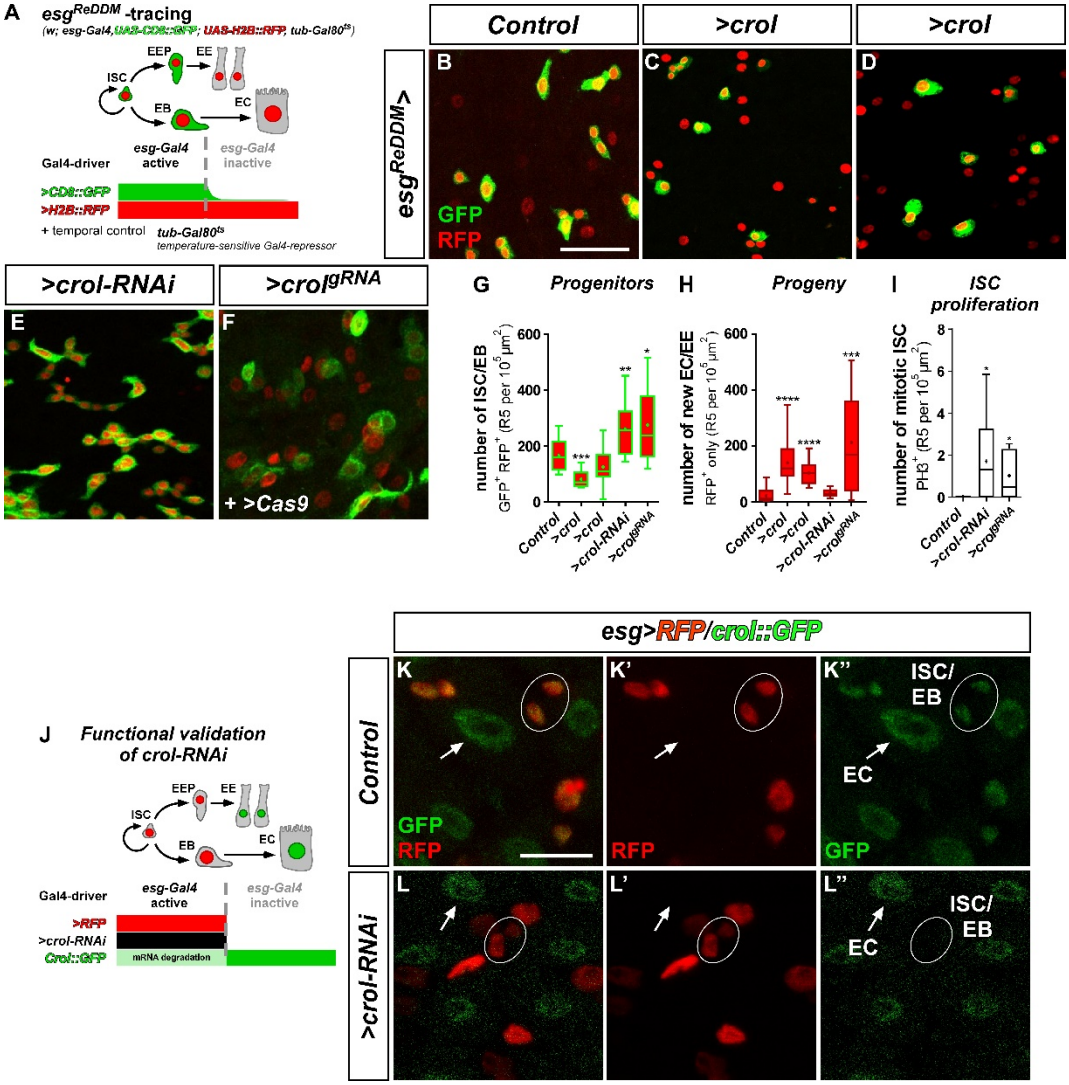

Fig.S2: Crol controls ISC proliferation and intestinal homeostasis

(A) Schematic of *esg*^{ReDDM} tracing. *esg-Gal4*, active in progenitor cells, double marks ISC/EB driving expression of *>CD8::GFP* (membrane, green) and *>H2B::RFP* (nuclei, red). Upon differentiation new epithelial EC and EE lose CD8::GFP signal, whereas nuclear H2B::RFP persists due to its long half-life enabling tracing of ISC/EB progeny. Transgene expression is timely controlled by an ubiquitously expressed temperature sensitive Gal80 repressor (*tub-Gal80*^{ts}). (B-F) Confocal images of adult midguts after seven days of *esg*^{ReDDM} tracing in (B) controls, OE of *crol* using two other overexpression lines: (C) Bloomington line BL58359 and (D) BL56762, (E) KD of *crol* using another RNAi-line: BL44643, and (F) knockout (KO) of *crol* induced by a *crol* guide RNA transgene (*>crol*^{gRNA}) consisting of two single gRNAs binding *crol* cDNA for CRISPR/Cas9 induced KO by *>Cas9*. Scale bar is 50µm. (G-I) Quantifications of (G) progenitor cell numbers (n=15,11,15,12,8), (H) progeny (n=15,11,15,12,8), and (I) ISC proliferation encompassing number of mitotically active ISC positive for aPH3 staining (n=8,9,5). Mean is indicated by (+) and asterisks denote significances from student's t-test (*p<0.05, **p<0.01, ***p<0.001, ****p<0.0001). (J) Schematic of a model for functional validation of *>crol-RNAi* and *crol::GFP* transgenes. Crol::GFP shows presence of Crol protein in all cell types and is combined with *esg-Gal4* driving expression of *>RFP* and *>crol-RNAi* in ISC/EB. Expression of *>crol-RNAi* leads to mRNA degradation within ISC/EB resulting in the subsequent loss of Crol::GFP signal. (K-L'') Confocal images of adult midguts with *crol::GFP* and *esg>RFP* in (K-K'') controls and (L-L'') combined with

>crol-RNAi resulting in visible loss of Crol::GFP signal within ISC/EB (outlined with white ellipses). White arrowheads point to EC that are positive for Crol::GFP signal in both conditions. Scale bar is 10µm.

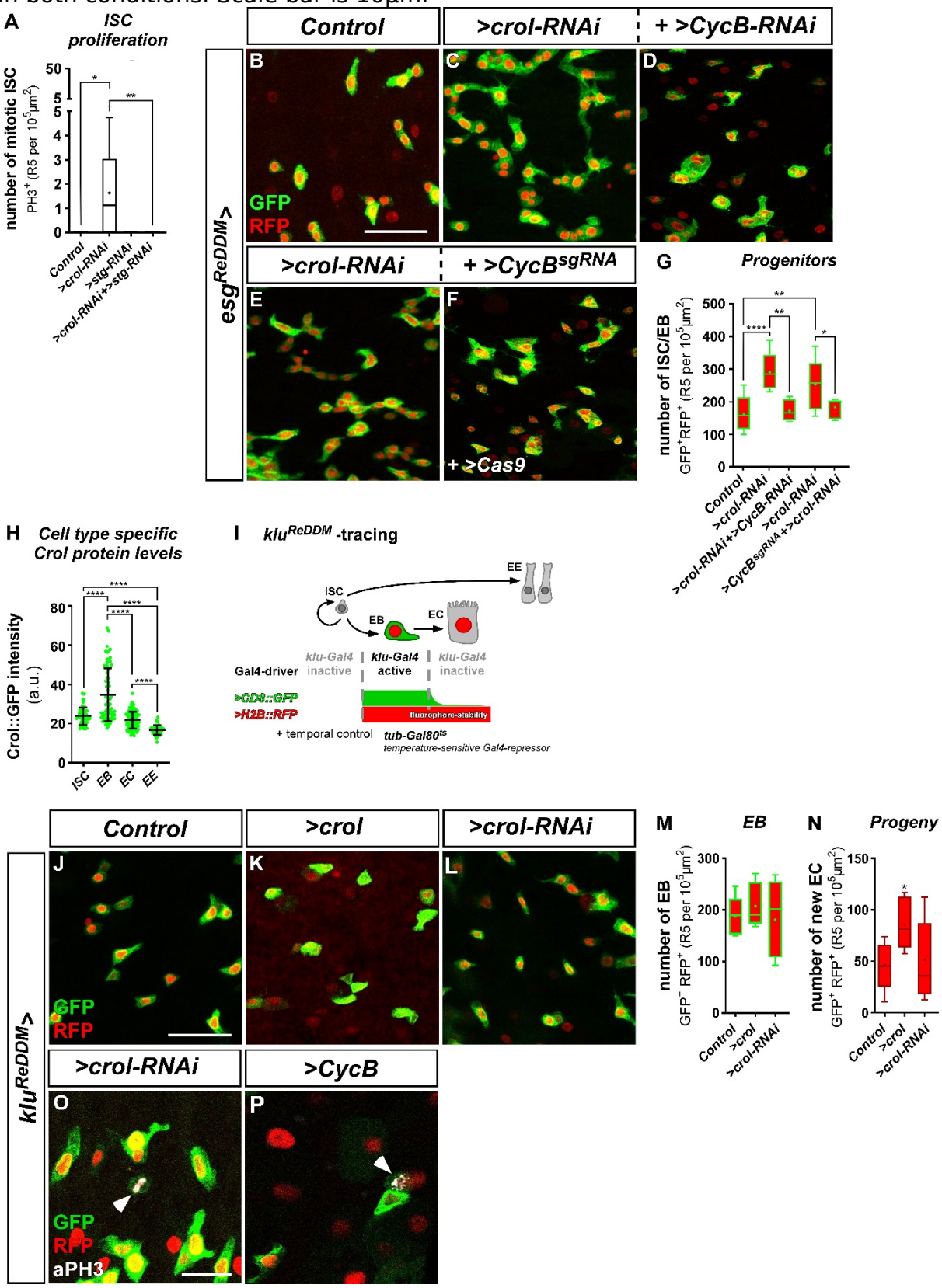

Fig.S3: Crol controls proliferation in ISC and EB by regulating CycB

(A) Quantification of mitotic ISC upon KD of *stg* and *crol* in *esg*^{ReDDM} traced for seven days (n=8,15,5,9). (B-F) Confocal images of adult midguts after seven days

of *esg*^{ReDDM} tracing in (B) controls, (C) upon expression of *>crol-RNAi* (D) combined with *>CycB-RNAi*, and (E) *>crol-RNAi* (F) combined with *>CycB*^{sgRNA} and *>Cas9* for CRISPR/Cas9 induced KO. Scale bar is 50µm. (G) Quantification of progenitor cell numbers in *esg*^{ReDDM} specific manipulations traced for seven days (n=13,8,4,10,6). (H) Quantification of Crol protein levels within different cell types of adult midguts indicated by Crol::GFP intensities (n=63,77,115,40). Means and standard deviations are visualized by vertical lines and asterisks denote significances from student's t-test (****p<0.0001). (I) Schematic of *klu*^{ReDDM} tracing. *Klu-Gal4*, active in EB, double marks EB driving expression of *>CD8::GFP* (membrane, green) and *>H2B::RFP* (nuclei, red). Upon differentiation new epithelial EC lose CD8::GFP signal, whereas nuclear H2B::RFP persists due to its long half-life enabling tracing of EB progeny. ISC and EE are not labelled/traced by fluorophores. Transgene expression is timely controlled by an ubiquitously expressed temperature sensitive Gal80 repressor (*tub-Gal80*^{ts}). (J-L) Confocal images of adult midguts after seven days of *klu*^{ReDDM} tracing in (J) controls, (K) *>crol*, and *>crol-RNAi*. Scale bar is 50µm. (M-N) Quantifications of (M) EB numbers and (N) progeny upon seven days of *klu*^{ReDDM} specific manipulation and tracing (n=7,6,9/7,6,9). Means are indicated by (+) and asterisks denote significances from student's t-test (*p<0.05). (O-P) Confocal images of midguts after seven days of *klu*^{ReDDM} tracing driving expression of (O) *>crol-RNAi* and (P) *>CycB*. Mitotically active EB are visualized by aPH3 staining. Scale bar is 20µm.

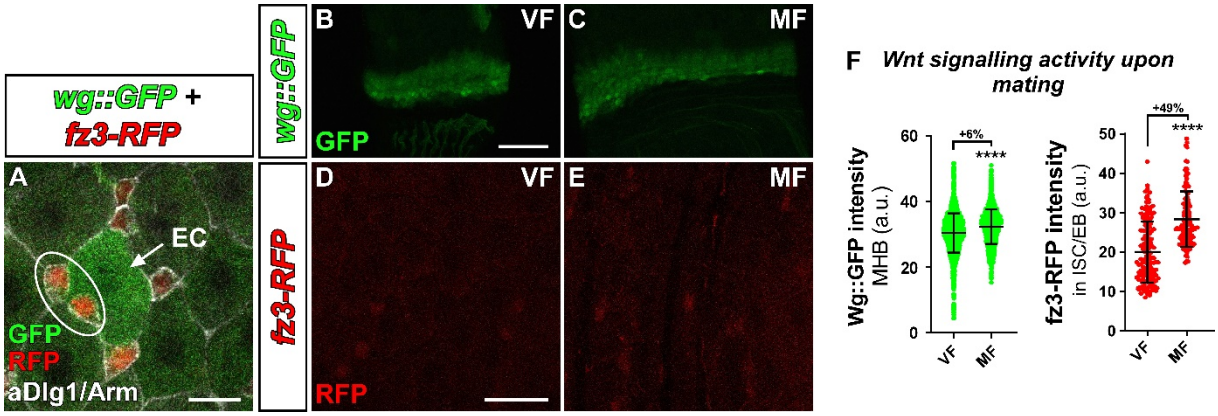

Fig.S4: Wnt/Wg activity in ISC/EB responds to mating dependent 20HE release

(A) Confocal image of *wg::GFP* combined with *fz3-RFP* in adult midgut showing Wg::GFP signal in EC marked by aDlg1 staining (white arrow) and fz3-RFP signal in surrounding ISC/EB stained by aArm and outlined by white ellipse. Scale bar is 10µm. (B-C) Confocal images of Wg::GFP in midgut-hindgut boundaries (MHB) of (B) VF and (C) MF. Scale bar is 50µm. (D-E) Confocal images of fz3-RFP in midguts of (D) VF and (E) MF flies. Scale bar is 20µm. (F) Quantifications of Wg::GFP levels in MHB and fz3-RFP levels in ISC/EB upon mating (n=5229,5660/150,129). Fold changes are shown in percentages, means and standard deviations are indicated by vertical lines and asterisks denote significances from student's t-test (****p<0.0001).

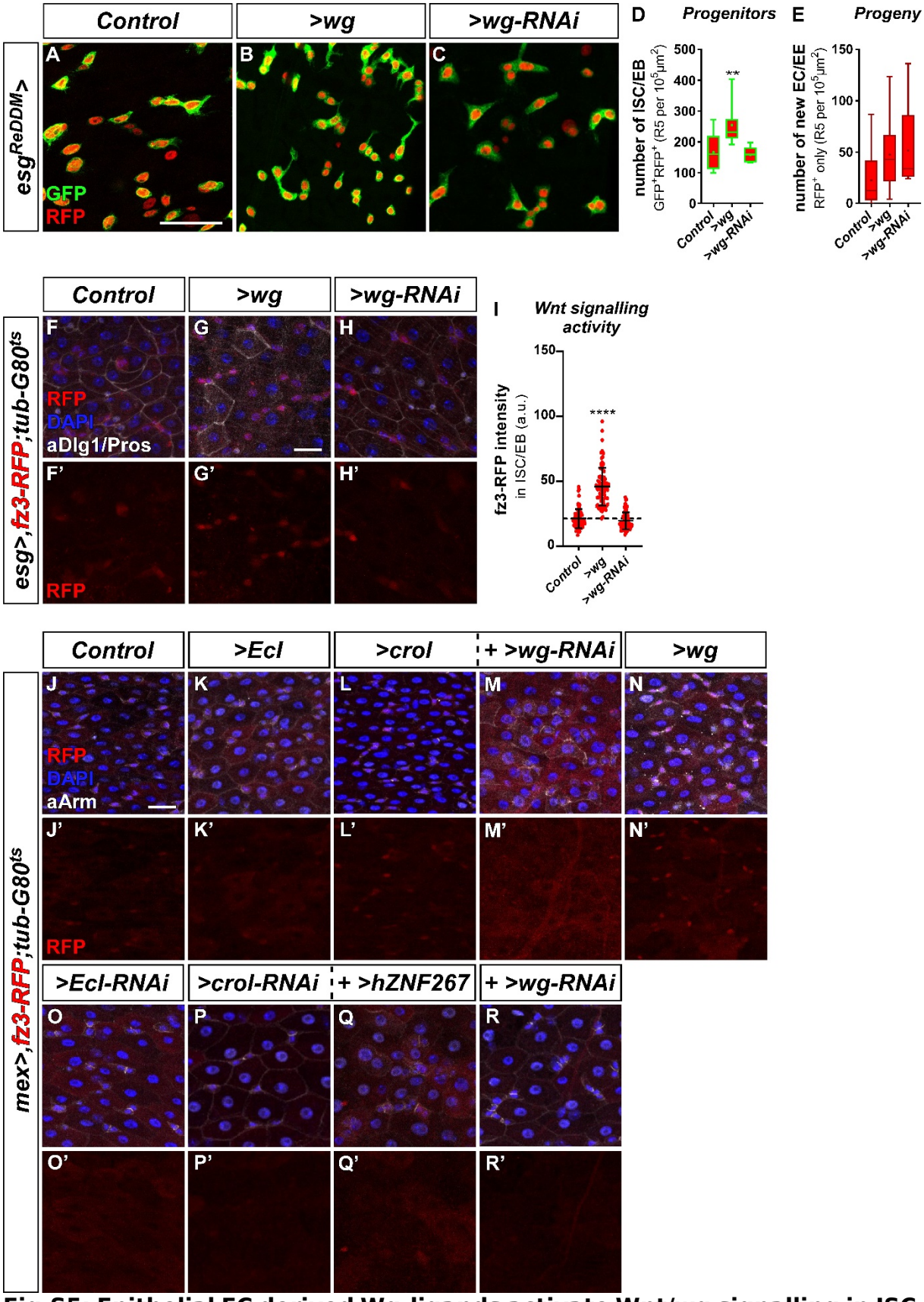

Fig.S5: Epithelial EC derived Wg-ligands activate Wnt/wg signalling in ISC
(A-C) Confocal images of adult midguts after seven days of *esg*^{ReDDM} tracing in (A) controls, upon (B) OE, and (C) KD of *wg*. Scale bar is 50µm. (D-E) Quantifications of (D) progenitor cell number and (E) progeny upon ISC/EB specific manipulations

of *wg* (n= 15,7,5/15,7,5). Means are indicated by (+) and asterisks denote significances from student's t-test (**p<0.001). (F-H') Confocal images of *fz3-RFP* combined with *esg-Gal4* and *tub-Gal80^{ts}* in adult midguts after three days of shifting in (F-F') controls, combined with ISC/EB specific (G-G') OE, and (H-H') KD of *wg*. EC and EE are marked by antibody staining against Dlg1 and Pros. Scale bar is 20µm. (I) Quantification of fz3-RFP levels in ISC/EB upon *esg-Gal4* specific *>wg* and *>wg-RNAi* (n=90,90,90). Means and standard deviations are indicated by vertical lines and asterisks denote significances from student's t-test (****p<0.0001). (J-R') Confocal images of *fz3-RFP* combined with *mex-Gal4* and *tub-Gal80^{ts}* in adult midguts after one day of shifting in (J-J') controls, EC specific OE of (K-K') *EcI*, (L-L') *croI* (M-M') with simultaneous KD of *wg*, and (N-N') *wg*, and KD of (O-O') *EcI*, (P-P') *croI* (Q-Q') with simultaneous expression of *>hZNF267*, and (R-R') *wg* in EC. ISC/EB are marked with anti-Armadillo (aArm) staining. Scale bar is 20µm.

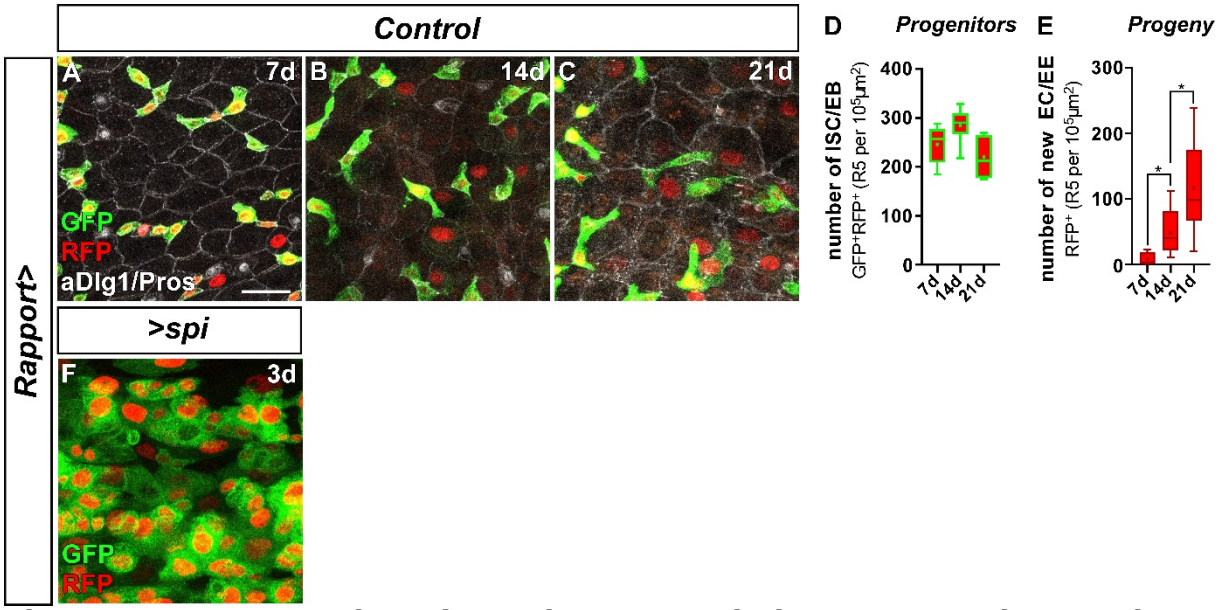

Fig.S6: Rapport tracing shows incremental tissue renewal over three weeks

(A-C) Confocal images of adult midguts with Rapport expression system in controls after (A) seven, (B) 14, and (C) 21 days of tracing showing GFP^+RFP^+ ISC/EB and their RFP^+ progeny. EC and EE are marked by anti-Dlg1 and aPros staining. Scale bar is 20µm. (D-E) Quantifications of (D) progenitor cell number and (E) progeny in control midguts upon seven, 14 and 21 days (7d, 14d, 21d) of tracing (n=5,7,7/5,7,7). Means are indicated by (+) and asterisks denote significances from student's t-test (*$p<0.05$). (F) Confocal image of an adult midgut after three days of Rapport tracing and EC specific OE of *spitz* (*>spi*).

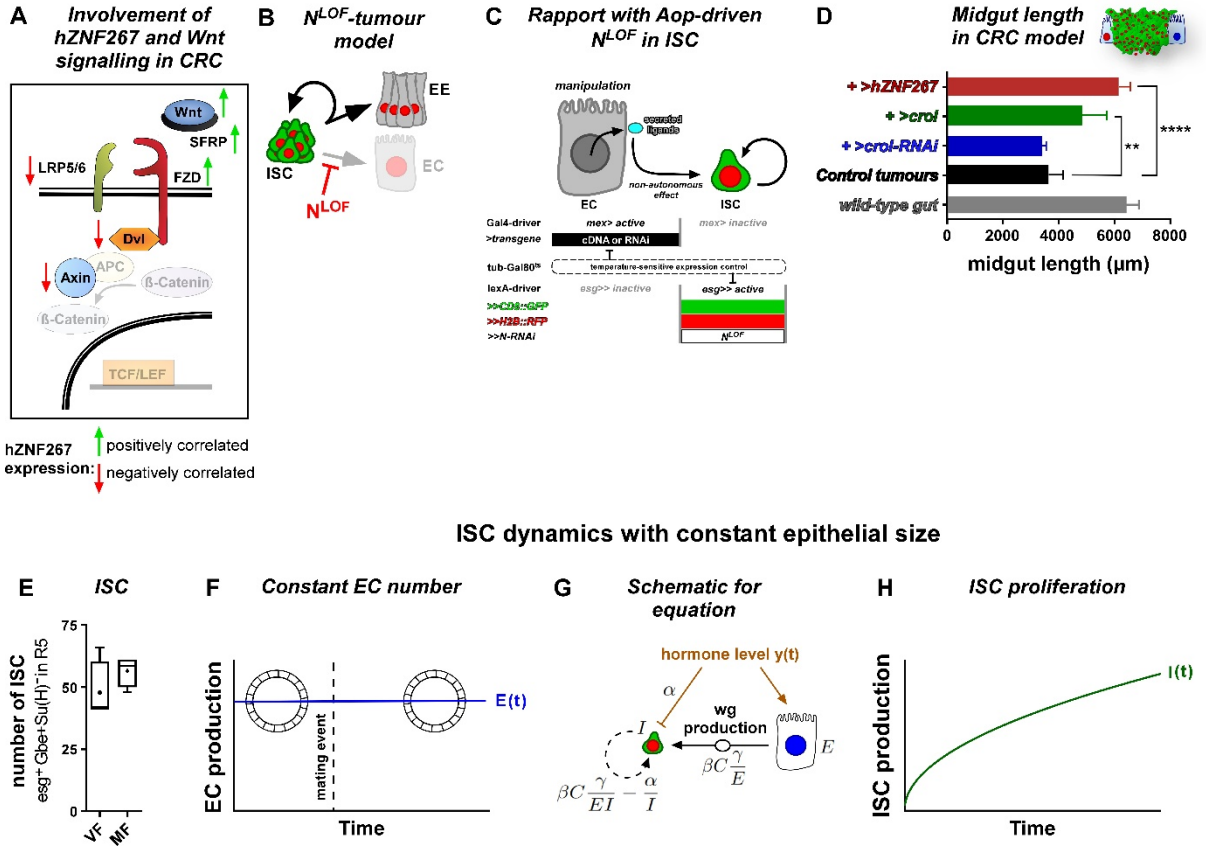

Fig.S7: Additional data for tumour and mathematical modelling

(A) Schematic of the involvement of ZNF267 and Wnt signalling in CRC. Wnt ligand is bound by secreted frizzled related proteins (SFRP) preventing binding to the frizzled receptor (FZD) and its co-receptors LDL receptor related protein 5 and 6 (LRP5/6). Dishevelled segment polarity protein 1 (DVL) forms a complex with both receptors and recruits the destruction complex consisting of APC and axin 1 (AXIN) which degrade cytoplasmic ß-Catenin thereby preventing its translocation to the nucleus and binding to transcription factors of the TCF/LEF family. Marked with green arrows are components that positively correlate with enhanced ZNF267 expression in CRC, whereas components with negative correlation of expression are marked with red arrows. (B) Schematic of the N^{LOF}tumour model. N^{LOF} in ISC blocks differentiation into EC inducing the formation of ISC and EE tumours. (C) Schematic of the combination of *Rapport* with a N^{LOF}-tumour model. *Rapport* consist of a *mex-Gal4* driver enabling EC specific expression of UAS-driven cDNAs or RNAi constructs and an *esg^{lexReDDM}* system based on lexA/Aop allowing Gal4/UAS independent labelling and tracing of ISC/EB by *esg-lexA* driven expression of *Aop-CD8::GFP* and *Aop-H2B::mCherry* and additional expression of *Aop-N-RNAi* for induction of N^{LOF} within ISC (lexA/Aop abbreviated as '>>' hereafter), both expression systems are timely controlled by a *tub-Gal80^{ts}* repressor. (D) Quantification of midgut length as a readout for epithelial deterioration in a CRC model combined with ISC/EB specific manipulations of *crol*/ZNF267 (n=14,7,8,5,5). Column bars show means with standard deviations and asterisks denote significances from student's t-test (**p<0.01, ****p<0.0001). (E) Quantification of ISC numbers in VF compared to MF (n=4,4). Mean is indicated by (+). (F-H) Function showing ISC dynamics with constant epithelial size. (F) Function visualizing constant EC number resulting in constant intestinal size depicted by gut sections. (G) Schematic for equation visualizing the divergent effect of 20HE hormone on ISC (I) inhibiting ISC proliferation and on EC (E) stimulating Wg production $\beta C\frac{\gamma}{E}$. In a situation with blocked EC differentiation ISC proliferation

increases with $\beta c\frac{\gamma}{EI} - \frac{\alpha}{I}$. (H) Function showing ISC proliferation $I(t)$over time in a situation of constant EC number.

Figures

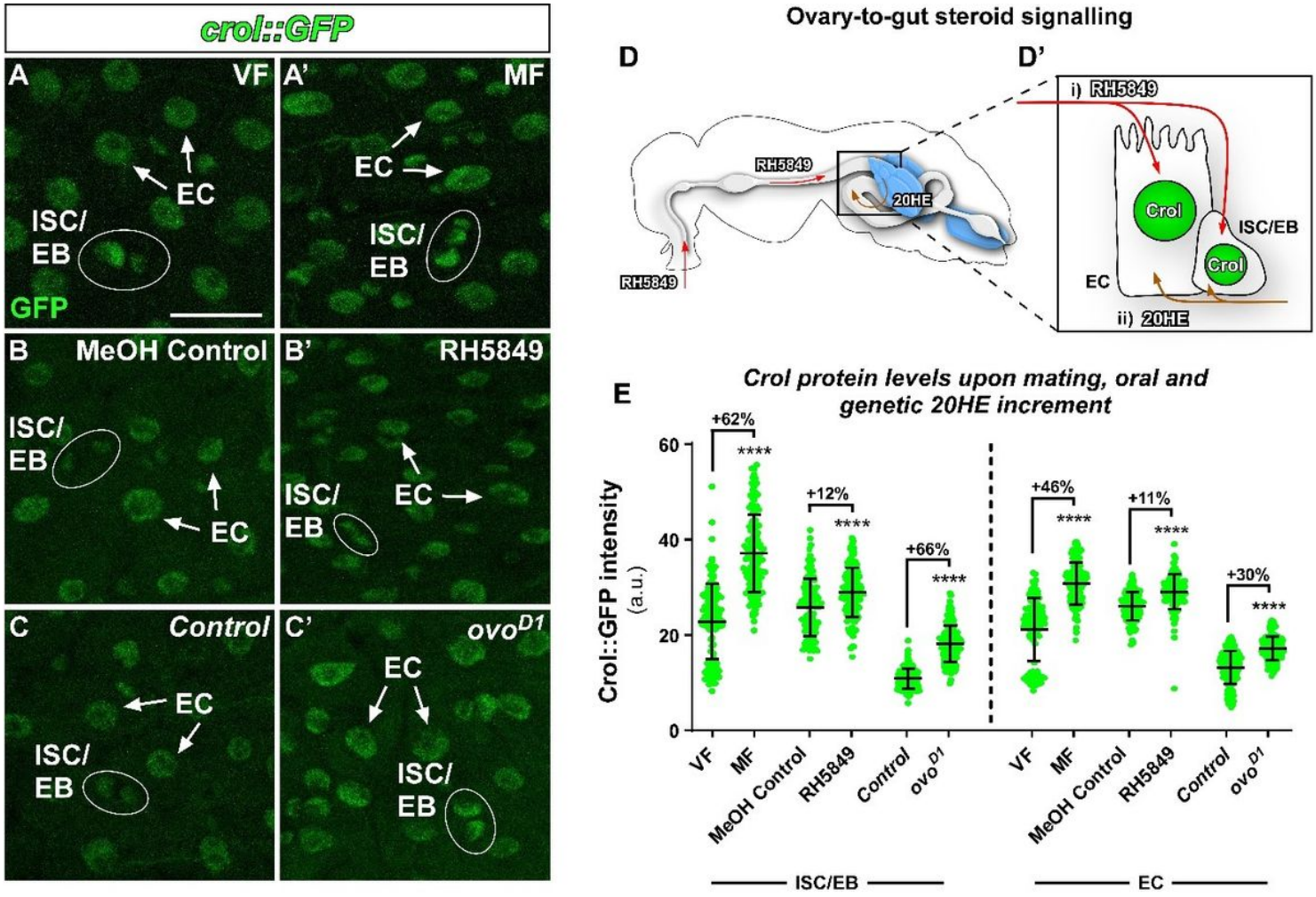

Fig.1: Crooked legs responds to 20HE steroid hormone release

(A-C') Confocal images showing GFP-tagged crooked legs (Crol::GFP) in adult midguts of (A) virgin female (VF) flies compared to (A') mated female (MF) flies, (B) MF fed with MeOH (MeOH Control) compared to (B') MF fed with 20HE agonist RH5849 diluted in MeOH, and (C) MF w^{1118} flies (Contol) compared to (C') heterozygous ovo^{D1} mutant MF. Duplets of stem- and progenitor cells (ISC/EB) are outlined by white ellipses and EC are marked with white arrows. Scale bar is 20µm. (D-D') Schematic of a female fly including midgut and ovaries. The 20HE agonist RH5849 is administrated orally and i) absorbed from the midgut lumen into ISC/EB and EC, whereas 20HE is produced in ovaries and released into the hemolymph ii) from where it is imported into midgut cells. (E) Quantifications of Crol::GFP intensities in ISC/EB and EC upon 20HE levels increased by mating (VF compared to MF), oral administration of 20HE agonist RH5849 (MeOH Control compared to RH5849), and genetical ablation of ovaries by ovo^{D1} mutant allele (*Control* compared to ovo^{D1}). Fold changes are shown in percentages, means and standard deviations are indicated by vertical lines (n=120,120,78,91,178,168/120,120,78,91,198,168). Asterisks denote significances from student's t-test (**p<0.01, ****p<0.0001).

Figure 1

See image above for figure legend.

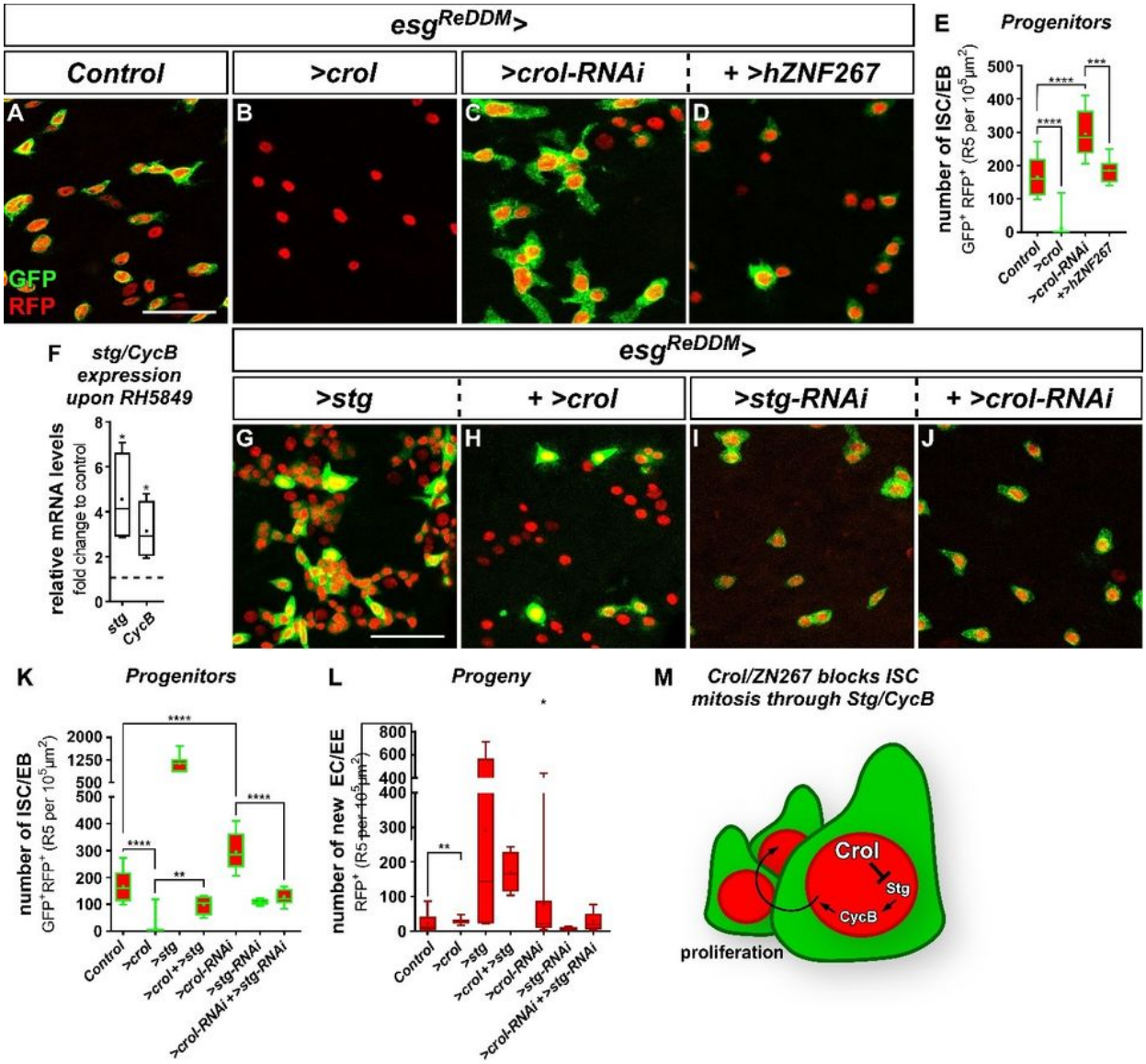

Fig.2: Crol and ZNF267 control ISC proliferation through String/Cyclin B

(A-C) Confocal images of adult female midguts after seven days of *esg*^{ReDDM} tracing showing (A) controls with active *esg-Gal4* in ISC/EB driving expression of *UAS-CD8::GFP* (membrane GFP) and *UAS-H2B::RFP* (nuclear RFP), and newly differentiated epithelial cells with inactive *esg-Gal4* are RFP+-only owing to protein stability of H2B::RFP, (B) ISC/EB specific overexpression (OE) of *UAS-crol* (UAS abbreviated as '>' hereafter in figure panels), (C) knockdown (KD) of *crol* by *>crol-RNAi*, and (D) simultaneous expression of the human Crol orthologue ZNF267 (*>hZNF267*). Scale bar is 50µm. (E) Quantification of progenitor cell numbers encompassing ISC and EB (n=9,10,15,12). Mean is indicated by (+) and asterisks denote significances from student's t-test (***p<0.001, ****p<0.0001). (F) Quantitative RT-PCR on intestinal cDNA from MF fed with 20HE agonist RH5849 showing relative mRNA levels of *string* (*stg*) and *Cyclin B* (*CycB*) (n=4,4). Values are normalized to MeOH control. (G-J) Confocal images of adult female midguts after seven days of *esg*^{ReDDM} tracing showing (G) ISC/EB specific OE of *stg* (H) combined with *>crol*, and (I) specific KD of *stg* by RNAi, (J) combined with *>crol-RNAi*. Scale bar is 50µm. (K-L) Quantifications of (K) progenitor cell numbers and (L) progeny (n=9,10,7,4,15,5,9/9,10,7,4,15,5,9). Mean is indicated by (+) and asterisks denote significances from student's t-test (*p<0.05, **p<0.01, ****p<0.0001). (L) Schematic showing inhibition of Stg and CycB by Crol within ISC thereby controlling proliferation.

Figure 2

See image above for figure legend.

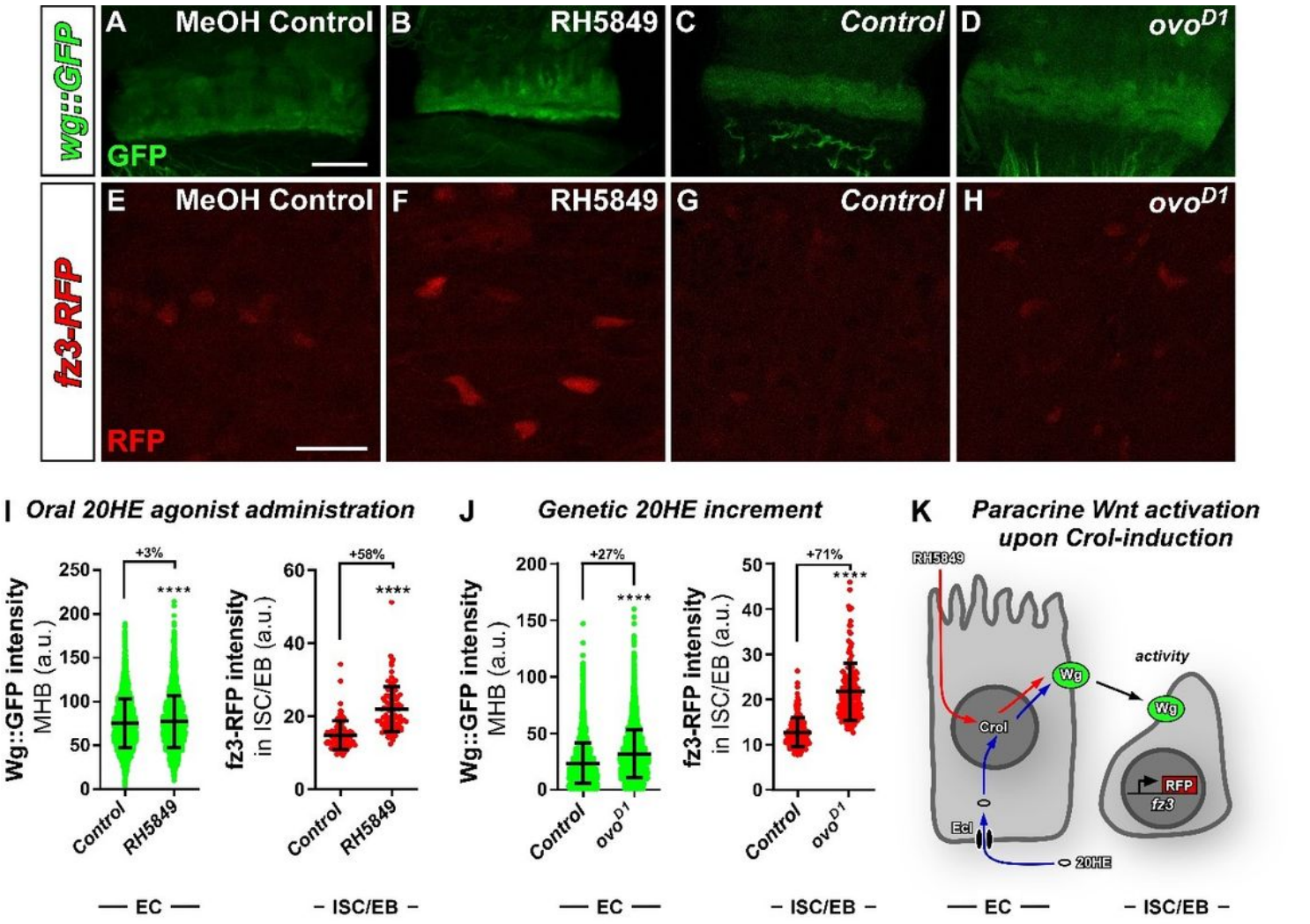

Fig.3: 20HE induced wg ligands from EC activate Wnt/wg signalling in ISC

(A-D) Confocal images of GFP-tagged Wnt ligand wingless (*wg::GFP*) in adult midguts of (A) MF fed with MeOH (MeOH Control) compared to (B) MF fed with 20HE agonist RH5849, and (C) control flies compared to heterozygous ovo^{D1} mutant MF. Scale bar is 50µm. (E-H) Confocal images of adult midguts with RFP expressed under control of the fz3 promotor (*fz3-RFP*) as readout for Wnt activity in (E) controls compared to (F) flies fed with RH5849, and (G) controls compared to (H) heterozygous ovo^{D1} mutant flies. Scale bar is 20µm. (I-J) Quantifications of Wg::GFP intensities in EC and fz3-RFP intensities in ISC/EB upon (I) oral administration of 20HE agonist RH5849 and (J) genetic 20HE increment upon ablation of ovaries. Fold changes are shown in percentages, means and standard deviations are indicated by vertical lines (n=7595,5192/90,90/8646,10874/178,168). Asterisks denote significances from student's t-test (****p<0.0001). (K) Schematic of paracrine Wnt/wg activation upon 20HE increment. RH5849 is incorporated into EC from the midgut lumen, whereas 20HE from surrounding hemolymph is imported into EC by the ecdysone importer (Ecl). Within EC the hormone or its agonist activate expression of *crol*, and expression of *wg*. Wg ligand is then secreted by the EC and non-autonomously activates Wnt/Wg signalling in ISC visible by expression of fz3-RFP.

Figure 3

See image above for figure legend.

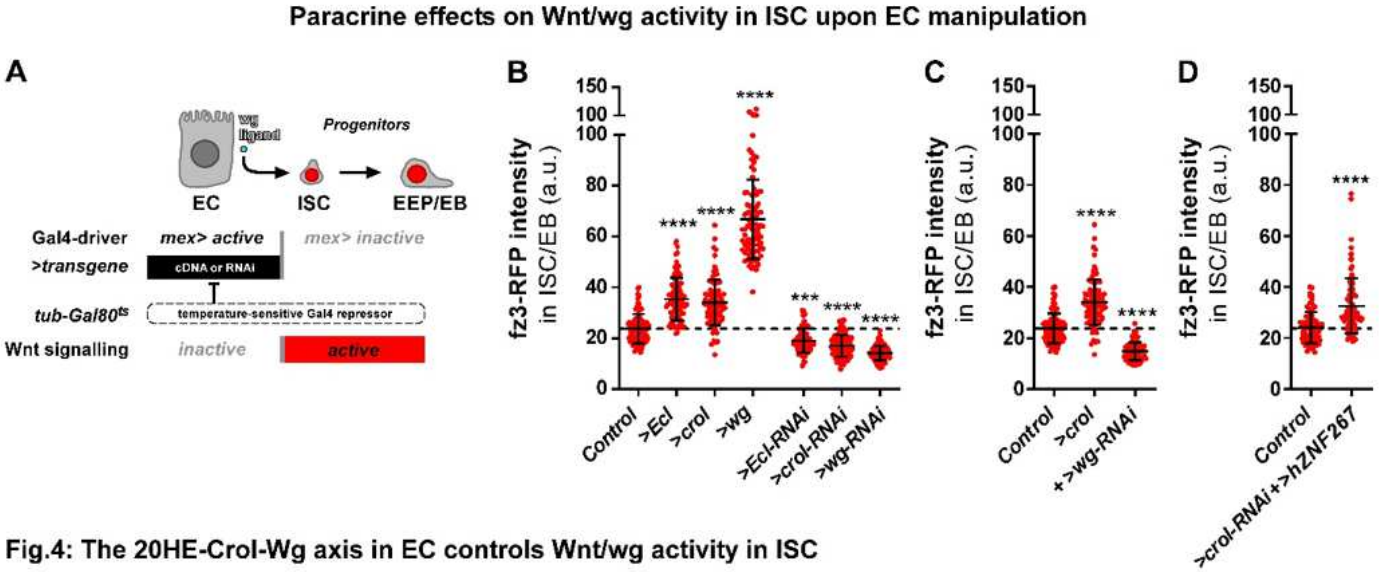

Fig.4: The 20HE-Crol-Wg axis in EC controls Wnt/wg activity in ISC

(A) Schematic of a system enabling EC manipulation and simultaneous visualization of Wnt/Wg activity in ISC/EB. *mex-Gal4* is active in EC and allows specific manipulation of EC by crossing to UAS-driven transgenes. These manipulations are timely controlled by an ubiquitously expressed temperature sensitive Gal4 repressor (*tub-Gal80^{ts}*) and combined with *fz3-RFP* sensor reflecting Wnt/Wg activity in ISC/EB independent of Gal4. (B-D) Quantifications of fz3-RFP intensities in ISC/EB with (B) OE and KD of *Ecl*, *crol* and *wg* (n=90,90,90,90,75,60,120), (C) EC specific OE of *crol* combined with *>wg-RNAi* (n=90,90,90), and (D) ectopic expression of *>hZNF267* in *crol* depleted EC (n=90,89). Means and standard deviations are indicated by vertical lines and asterisks denote significances from student's t-test (***p<0.001, ****p<0.0001).

Figure 4

See image above for figure legend.

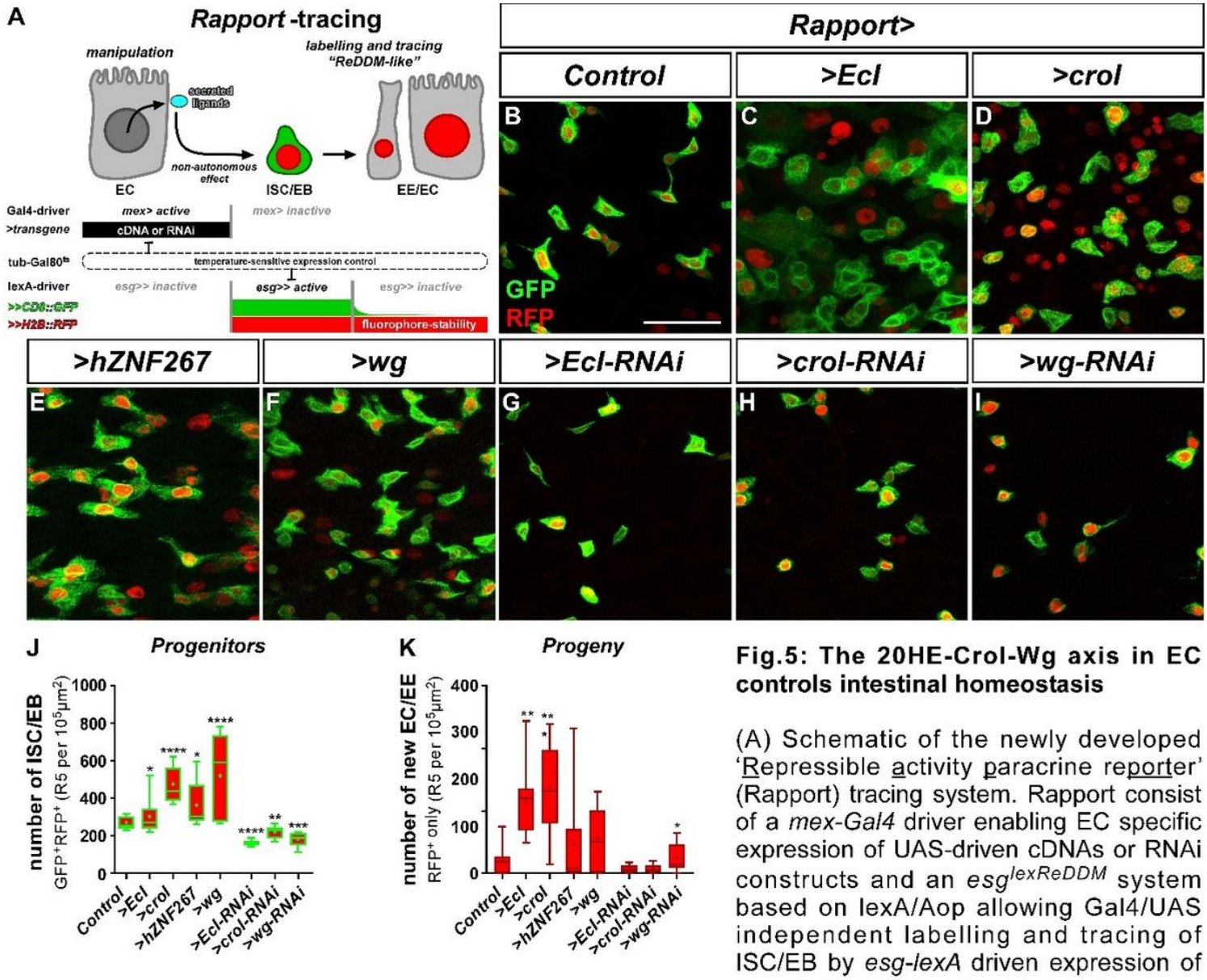

Fig.5: The 20HE-Crol-Wg axis in EC controls intestinal homeostasis

(A) Schematic of the newly developed 'Repressible activity paracrine reporter' (Rapport) tracing system. Rapport consist of a *mex-Gal4* driver enabling EC specific expression of UAS-driven cDNAs or RNAi constructs and an *esg*^{lexReDDM} system based on lexA/Aop allowing Gal4/UAS independent labelling and tracing of ISC/EB by *esg-lexA* driven expression of *Aop-CD8::GFP* and *Aop-H2B::mCherry* (lexA/Aop abbreviated as '>>' hereafter), both expression systems are timely controlled by a *tub-Gal80*^{ts} repressor. (B-I) Confocal images of adult midguts after (B,D-E,G-H) seven days or (C,F,I) 10 days of Rapport tracing of (B) controls, OE of (C) *Ecl*, (D) *crol*, (E) *hZNF267* and (F) *wg*, and KD of (G) *Ecl*, (H) *crol* and (I) *wg* showing GFP$^+$ and RFP$^+$ ISC/EB and their differentiated progeny labelled only by RFP. Scale bar is 50µm. (J-K) Quantifications of (J) progenitor cell numbers and (K) their progeny upon EC specific manipulations of *Ecl*, *crol*, *hZNF267* and *wg* (n=9,5,10,9,10,7,13,5/9,5,10,9,10,7,13,5). Mean is indicated by (+) and asterisks denote significances from student's t-test (*p<0.05, **p<0.01, ***p<0.001, ****p<0.0001).

Figure 5

See image above for figure legend.

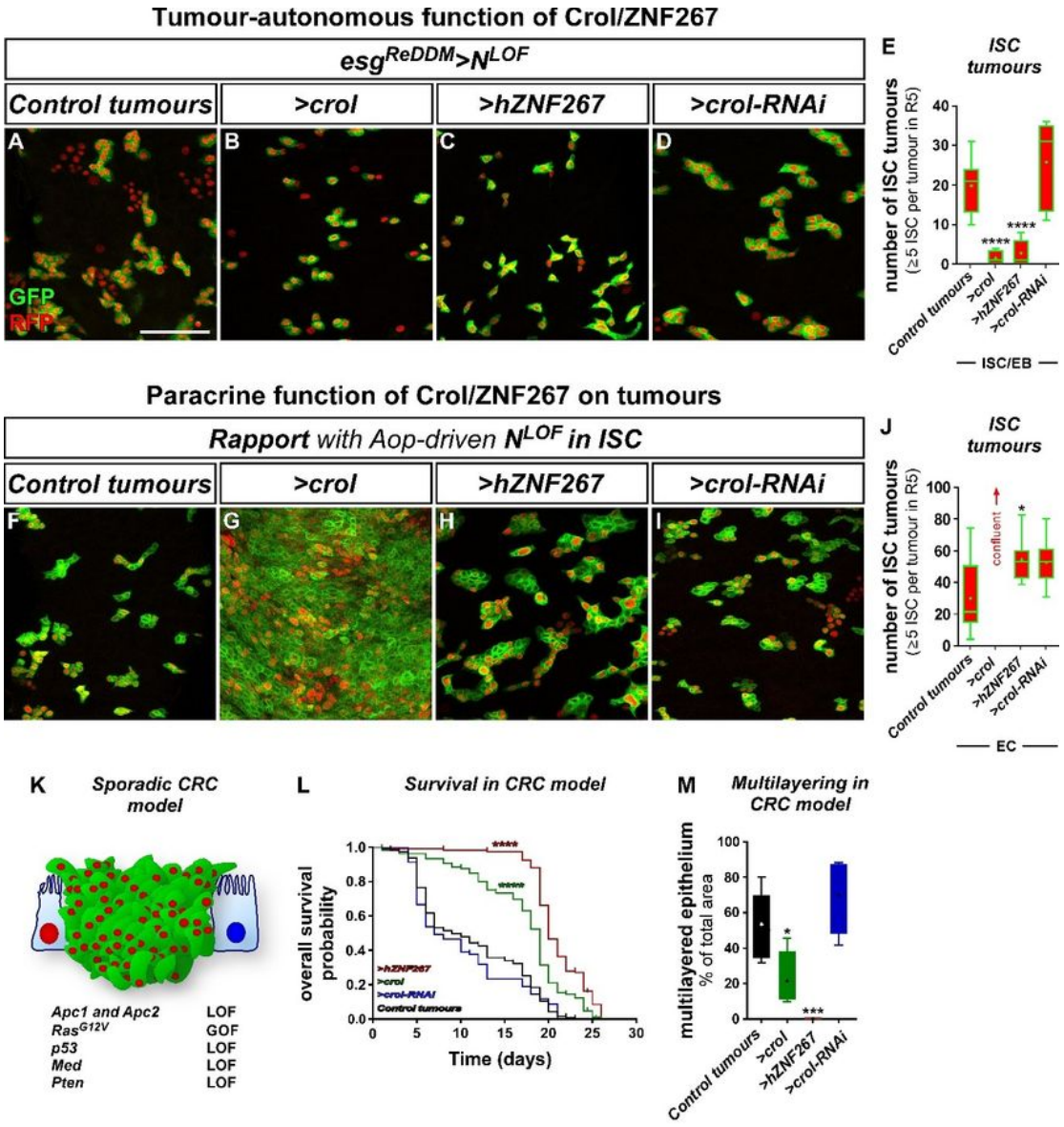

Fig.6: The mitotic balance of Crol/ZNF267 is preserved in intestinal tumour models

(A-D) Confocal images of adult midguts with ISC specific Notch loss of function (N^{LOF}) combined with esg^{ReDDM} tracing after three days of shifting in (A) controls, combined with (B) OE of *crol*, (C) expression of *>hZNF267*, and (D) *>crol-RNAi*. Scale bar is 50µm. (E) Quantification of ISC tumours encompassing number of clusters with 5 or more ISC (n=11,8,8,10). Mean is indicated by (+) and asterisks denote significances from student's t-test (****p<0.0001). (F-I) Confocal images of adult midguts with ISC specific N^{LOF} by expression of *Aop-N-RNAi* under control of *esg-lexA* within the Rapport tracing system after seven days of tracing in (F) controls, combined with EC specific (G) OE of *crol*, (H) expression of *>hZNF267*, and (I) *>crol-RNAi*. (J) Quantification of ISC tumours combined with EC specific manipulations of *crol*/*hZNF267* (n=10,-,10,10). Mean is indicated by (+) and asterisks denote significances from student's t-test (*p<0.05). (K) Schematic of a *Drosophila* CRC model combined with esg^{ReDDM} inducing formation of malignant tumours by ISC/EB specific expression of oncogenic *RasG12V* (gain of function, GOF) and CRISPR/Cas9 induced KO of *Apc1, Apc2, p53, Med,* and *Pten* (loss of function, LOF). (L) Kaplan-Meier estimation of survival in CRC model combined with manipulations of *crol*/*hZNF267* (n=119,121,118,69). Asterisks denote significances from Kaplan-Meier analysis (****p<0.0001). (M) Quantification of multilayered tissue encompassing percentage of area with intact EC indicated by anti-Dlg1 staining (n=7,4,4,7). Mean is indicated by (+) and asterisks denote significances from student's t-test (*p<0.05, ***p<0.001).

Figure 6

See image above for figure legend.

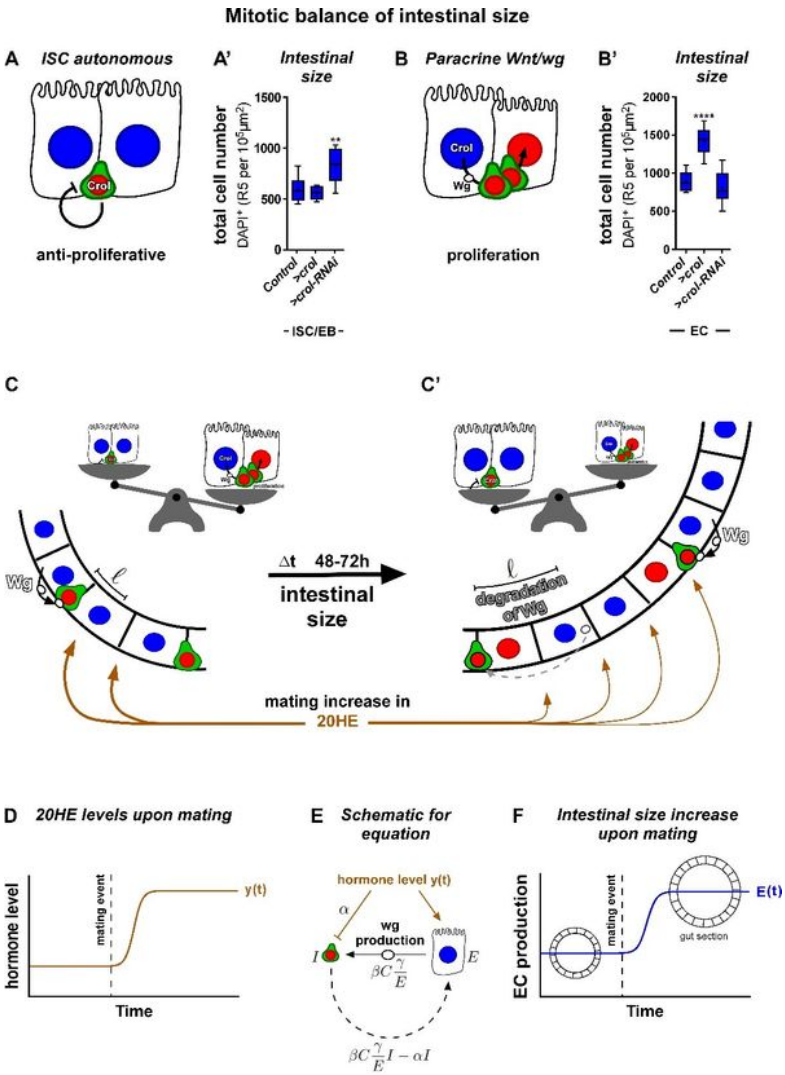

Fig.7: Mathematical modelling of hormone level controlled intestinal size

(A) Schematic of ISC autonomous function of Crol inhibiting ISC proliferation. (A') Quantification of intestinal size encompassing total cell number upon ISC/EB specific manipulations of *crol* (n=13,8,8). (B) Schematic of paracrine Wnt/wg release in EC regulated by Crol and inducing ISC proliferation. (B') Quantification of intestinal size encompassing total cell number upon EC specific manipulations of crol (n=9,10,17). Mean is indicated by (+) and asterisks denote significances from student's t-test (**p<0.01), ****p<0.0001). (C) Schematic of a gut section showing EC that release Wg ligand upon mating increase in 20HE signalling. Secreted Wg reaches ISC with a distance of ℓ. In a growing organ the function of Crol in inducing proliferation dominates the anti-proliferative function. (C') Upon an increase in intestinal size within 48-72h resulting in increasing EC number and thereby an increase in the average distance ℓ of EC (Wg source) and the ligand receiving ISC. With a longer distance ℓ Wg ligand degrades leading to a decrease in Wg concentration sensed by ISC and thereby to a decline in ISC proliferation. (D) A graph showing 20HE levels upon mating as a function ($\gamma(t)$) of hormone level per time. (E) Schematic for equation visualizing the divergent effect of 20HE hormone on ISC (I) inhibiting ISC proliferation and on EC (E) stimulating Wg production $\beta C\frac{\gamma}{E}$. Secreted Wg ligand stimulates ISC (I) to produce more EC (E) $\beta C\frac{\gamma}{E}I-\alpha I$. (F) A graph visualizing intestinal size increase upon mating as a function ($E(t)$) of EC production per time with a growing gut section following the mating event indicating intestinal growth.

Figure 7

See image above for figure legend.

Supplementary Files

This is a list of supplementary files associated with this preprint. Click to download.

- SupplementalFigures.docx
- NatureCellBiologyZipperetalMaterialandMethods.pdf
- NatureCellBiologyZipperetalmathmodel.pdf
- NatureCellBiologyZipperetalmathmodel.pdf